

**OPTICAL GENERATION OF TONE-BURST RAYLEIGH
SURFACE WAVES FOR NONLINEAR ULTRASONIC
MEASUREMENTS**

A Thesis
Presented to
The Academic Faculty

by

Christian B. Swacek

In Partial Fulfillment
of the Requirements for the Degree
Master of Science in
Engineering Science and Mechanics

School of Civil and Environmental Engineering
Georgia Institute of Technology
December 2012

OPTICAL GENERATION OF TONE-BURST RAYLEIGH
SURFACE WAVES FOR NONLINEAR ULTRASONIC
MEASUREMENTS

Approved by:

Professor Laurence J. Jacobs, Advisor
School of Civil and Environmental
Engineering
Georgia Institute of Technology

Dr. Jin-Yeon Kim
School of Civil and Environmental
Engineering
Georgia Institute of Technology

Professor Reginald DesRoches
School of Civil and Environmental
Engineering
Georgia Institute of Technology

Date Approved: August 23 2012

ACKNOWLEDGEMENTS

This thesis completes one year of research and studies as an exchange student in Atlanta, Georgia. My time at the Georgia Institute of Technology was rich in both valuable personal and professional experiences. These experiences would not have been possible on my own and without the support of others. First of all I would like to thank my advisor Prof. Laurence J. Jacobs who guided and supported me in both academic as well as personal affairs during my stay in Atlanta. His financial and organizational commitment also allowed me to attend the QNDE conference in Denver, Colorado, where I was able to present the results of this thesis. Furthermore, I would like to express my highest esteem and gratitude to Dr. Jin-Yeon Kim who was always willing to share his extraordinary knowledge and experience in ultrasonics with me. His courage and advice always guided me and motivated me in my progress. I want to thank Prof. Reginald DesRoches for serving as a committee member. I thank the Georgia Tech Invention Studio and Matthew Marchese for all the support for the fabrication of my equipment. Moreover, I am grateful to Prof. Lothar Gaul for choosing me as a candidate for the ISAP Program. In addition I would like to thank Dr. Jan Herrmann for his valuable advice and help during the preparation for the exchange program. I would like to acknowledge the DAAD (German Academic Exchange Service) for providing generous financial support. I want to thank my fellow students and labmates Kathryn Matlack, Chi-Luen Huang, Johann Gross, and Daniel Zeitvogel for their friendship and support in every concern. Finally, I want to express my deepest gratitude to my parents and my family and friends who always supported and encouraged me since the beginning when I applied for the exchange and continuously throughout my whole stay.

TABLE OF CONTENTS

ACKNOWLEDGEMENTS	iii
LIST OF TABLES	vi
LIST OF FIGURES	vii
LIST OF SYMBOLS	xiii
SUMMARY	xiv
I INTRODUCTION	1
1.1 Motivation and Objective	1
1.2 Literature Review	2
1.3 Content and Structure of the Thesis	3
II INTRODUCTION INTO WAVEPROPAGATION	5
2.1 Wave Phenomena	5
2.1.1 Equation of Motion	5
2.1.2 Plane Waves	8
2.2 Bulk and Surface Waves	8
2.2.1 Rayleigh Waves	11
2.3 Nonlinear Wave Theory	12
2.3.1 Nonlinear Wave Equation	13
III LASER ULTRASONICS	18
3.1 Non-contact Methods	19
3.2 Laser Generation Methods	19
3.2.1 Laser	20
3.2.2 Absorption of Electromagnetic Radiation	24
3.2.3 Temperature Distribution	26
3.2.4 Thermoelastic and Ablative Heat Source	28
3.2.5 Source Pattern Generation for Narrow Band Signal Excitation	34

3.2.6	Derivation of the Thermoelastic Source	41
3.2.7	Derivation of the Ablative Source	52
IV	EXPERIMENTAL SETUP	54
4.1	Laser	54
4.2	Diffraction Grating Set Up	55
4.3	Shadow Mask Set Up	57
4.4	Specimen	59
4.5	Signal Detection	60
4.6	Signal Processing	61
V	EXPERIMENTAL RESULTS	63
5.1	Harmonic Signal Generation	63
5.1.1	Signals Generated by Diffraction Optics	64
5.1.2	Signals Generated by Shadow Mask	67
5.2	Measurement of the Nonlinearity of materials	72
VI	CONCLUSION	77
	REFERENCES	82

LIST OF TABLES

4.1	Optics for diffraction and beam manipulation	58
4.2	Piezoelectric Transducers	61
5.1	Measurement of nonlinearity of the aluminum plate	74

LIST OF FIGURES

2.1	Traction force acting on a unit area with normal vector \mathbf{n}	6
2.2	Incident and reflected wave field for longitudinal (P)- and transversal (SV) waves in a unbounded half-space	10
2.3	Rayleigh surface wave schematic	12
2.4	Fatigue damage and acoustic detection	13
2.5	Higher harmonic excitation in nonlinear continua.	13
2.6	Schematic of current and reference configuration	14
3.1	Discrete energy level diagram for the stimulation principle.	22
3.2	Basics of the laser oscillator	23
3.3	Absorption of electromagnetic radiation and the resulting thermal and acoustic wave field[72]	25
3.4	Farfield pattern of compression wave by laser pulse[72]	29
3.5	Signal Amplitude of a) longitudinal wave, b) Rayleigh surface wave in aluminum as a function of incident pulse energy[6]	31
3.6	Signal Amplitude transversal wave in aluminum as a function of laser pulse energy[6]	32
3.7	Surface wave pulse shape for different excitation energies in the ablative regime[72]	33
3.8	Surface wave frequency spectrum for different excitation energies a) 0.5mJ b) 3mJ c) 3.5mJ by narrowband excitation with a pico second laser in the ablative regime[75]	34
3.9	Narrowband surface excitation by interference of two incident laser beams[75]	35
3.10	Narrowband surface excitation by a diffracted laser beam[40]	36
3.11	Narrowband surface excitation by lenticular array[20]	37
3.12	Narrowband surface excitation by illumination through a shadow mask[60] 38	38
3.13	Directivity of a laser line source ($4mm \times 1mm$) on mild steel[75]	38
3.14	Decrement of signal bandwidth with number of line sources[23]	39
3.15	Geometric principles of a diffraction grating[23]	40

3.16	Temporal and spatial Gaussian distribution of the laser beam for the 2-D case[8].	43
3.17	Surface element for the derivation of a infinite line source with reaction forces F_1^\pm due to thermal expansion and the excited Rayleigh wave R[4].	44
3.18	Surface element for finite point source[4].	46
3.19	Schematic superposition of force dipoles for a line source[8].	47
4.1	Illumination pattern for narrowband signal excitation by diffraction optics and different sets of focusing lenses. The signal is detected by a conventional wedge-transducer	56
4.2	a) Diffraction and focusing of laser beam for b) pattern of point sources by a spherical lens and c) pattern of line sources by a cylindrical lens	57
4.3	Illumination pattern for narrowband signal excitation by a shadow mask. The signal is detected by a conventional wedge-transducer . . .	59
4.4	5MHz Narrowband tone-burst signal by mask illumination	62
5.1	Measurement of Rayleigh wave speed on aluminum. Seven measurements with distance $\Delta s = 5\text{ mm}$	64
5.2	5 MHz Narrow band signal excitation by Beamsplitter on steel a) in focus, b) 1.5 mm out of focus, c) 5 mm out of focus.	65
5.3	5 MHz Narrow band signal excitation by Beamsplitter line focused on steel with a cylindrical lens.	66
5.4	5 MHz Signal excitation by Diffuser (no additional focusing optics). .	66
5.5	2 MHz signal excitation by shadow mask and a beam diameter of 6 mm.	67
5.6	5 MHz signal excitation by shadow mask and $\times 2$ expanded laser beam.	68
5.7	Averaged signal to increase signal to noise ratio	69
5.8	Ablation damage on steel a) for 1.) a single laser pulse, 2.) 256 pulses, 3.) 32 pulses. b) microscope picture (200 \times magnification of the damage after 256 pulses.	70
5.9	Excitation behavior of the first and second harmonic component against number of laser pulses on steel.	71
5.10	Excitation behavior of the first and second harmonic component against number of laser pulses on aluminum.	72
5.11	Development of the nonlinearity parameter and the first and second harmonic amplitudes on aluminum.	73

5.12	Nonlinearity measurment on aluminum averaged for different number of pulses.	74
5.13	Best linear fit for nonlinearity measurements showing similar slopes. .	75
5.14	Nonlinearity measurement on steel. Shown is the development of the nonlinearity parameter and the behavior of the first and second harmonic amplitude.	76

LIST OF SYMBOLS

Symbol	Description
A	Amplitude
A_1	Amplitude of first harmonic
A_2	Amplitude of second harmonic
A_V	Area
B_1, B_2	Amplitudes
c, c_n	Phase velocities
c_L	Phase velocity for longitudinal waves
c_R	Phase velocity for Rayleigh waves
c_S	Phase velocity for Transversal waves
c_v	Specific heat at constant deformation
C	Heat Capacity
\mathbf{C}	Fourth-order modulus tensor
C_{ijklmn}	Tensor of third order elastic constants
C_1, C_2	Constants
d	Array parameter
d_G	Characteristic width of a Gaussian distribution
D_1	Constant
D, \bar{D}	Force dipoles
\mathbf{f}	Body force
\mathbf{d}	Propagation direction
E	Pulse Energy
E_0, E_1, E_2	Discrete Energy levels
f, f_n	Frequency
f_a	Ablative force amplitude

Symbol	Description
F_1, F_r	Force
\mathbf{F}	Deformation gradient
$I, I' I''$	Radiation Intensities
I_c	Critical Intensity
k, k_n	Wave number
k_L	Longitudinal wave number
k_S	Transversal wave number
k_S	Rayleigh wave number
k^B	Boltzmann constant
K	Thermal conductivity
l, l_3	Dimensions of infinitesimal elements
L	Distance grating-specimen
N	Number of lines in a line array
N_i	Number of particles
p	Grating pitch
\mathbf{p}	Vector of in plane particle motion
\mathbf{P}	Piola Kirchoff tensor
q	Deposited heat
Q	Latent heat for vaporization
r_0	Finite point source radius
R	Reflectivity
R_G	Gaussian Beam Radius
\mathbf{t}	Traction vector
t	Time
T, T_0	Absolute temperatures
T_v	Vaporization Temperature

Symbol	Description
\mathbf{u}	Displacement vector
V	Body volume, half-plane Volume
w	Slit width
\mathbf{x}	= Lagrangian Coordinates
$[x_1, x_2, x_3]$	
\mathbf{X}	Eulerian Coordinates
α	Linear thermal expansion coefficient
β	Nonlinearity parameter
β_c	Thermoelastic coupling constant
γ	Absorption coefficient
δ	Skin depth
ϵ	Strain tensor
ζ	Rate of re-
	Incident, reflection, or diffraction angle
moved mate-	
rial θ_n	
θ_r	Critical angle
κ	Thermal diffusivity
λ_R	Rayleigh wave length
λ, μ	Lamé-constants
μ_r, μ_0	(relative) permeability
ν	Poisson's ratio
ν^r	Radiation frequency
ν^t	Laser pulse rise time parameter
ρ, ρ_0	Densities in current and reference configuration
σ	Conductivity
τ	Stress tensor

Symbol	Description
ϕ	Carrier wave
φ	Scalar potential function
ψ	Vector potential function
ω	Circular frequency

SUMMARY

Conventional contact ultrasonic methods suffer from large variability, which is known to originate from a number of sources such as coupling variability, and the surface roughness at the transducer/specimen interface. The inherently small higher-harmonic signals can be significantly influenced by the changes in contact conditions, especially in nonlinear ultrasonic measurements. For this reason, the noncontact generation and detection techniques are very attractive. This research first focuses on the optical generation of tone-burst surface acoustic waves in a metallic specimen. Two methods that use laser light as an optical source are compared for generating surface acoustics waves in the 5 MHz range. Both the shadow mask and diffraction grating are used to convert a laser pulse to a tone-burst signal pattern on the specimen. The generated signals are detected by a wedge transducer at a fixed location and then the harmonic contents in the generated signals and the repeatability of the methods are evaluated. Finally, the developed method is used to characterize the material nonlinearity of aluminum (Al 6061) and steel (A36). The results showed repeatable measurements for ablative signal excitation on aluminum.

CHAPTER I

INTRODUCTION

1.1 Motivation and Objective

Ultrasonics are used for the detection of structural and material damage and material characterization. Most of the linear ultrasonic techniques are suitable for the detection of cracks and flaws, thus they are limited to the detection of a macroscopic damage. Nonlinear ultrasonics have the potential to detect material damage prior to crack initiation and material failure. In the early state of damage, such as damage due to fatigue, creep, nuclear radiation and corrosion, crystallographic dislocations and substructural damage result in material nonlinearities. This nonlinearity causes higher harmonic components in originally monochromatic signals which can be detected in the frequency spectrum. For many technical applications surface damage due to the mechanisms mentioned above is a severe failure source and the detection in an early state is desirable. Rayleigh surface waves concentrate their acoustic energy near the surface and can propagate large distances without significant losses due to their nondispersive character. A common way to launch a surface wave is by contact excitation methods, such as the use of piezoelectric wedge-transducers. Those methods suffer from the variability introduced by the coupling conditions on the contact surfaces and coupling media, and influences on the generated and detected signal by the mechanical characteristics of the exciting device. However noncontact methods are to a great extent free of those influences and offer advantages in the applicability in the field, such as in-situ testing of operating dynamic systems and testing in hazardous and hostile conditions. During the last two decades, laser ultrasonic excitation principles have had growing application in the field and an extensive list of literature

for the application in linear acoustics is available. Until now there has been little attention for the use of thermoelastic and ablative excitation for nonlinear material investigations.

The objective of this research is to develop a reliable noncontact excitation technique for the measurement of the material's nonlinearity. The excitation is by radiation of a q-switched pulsed laser which has to be manipulated to enable a harmonic excitation. The excited narrowband signal has to satisfy the requirements for detectability of higher harmonic signal components by piezoelectric wedge transducers.

1.2 Literature Review

A common technique in the field of nondestructive evaluation is the use of ultrasonics[2, 31]. Linear ultrasonics can be used for the detection of flaws, cracks and the characterization of materials and material properties[77]. However, the sensitivity of linear evaluation techniques is limited to macro failures and damages while modern research strives forward to detect a defect in its development process before significant damage occurs. Many early damages, such as creep, fatigue or corrosion damage cause dislocations[37], plastic deformations [45] and micro cracks resulting in a nonlinear acoustic behavior of the material[17, 84, 11, 47, 66]. Common methods to excite and detect the acoustic signal for nonlinear ultrasonics is by using contact transducers [78, 50, 12] or hybrid techniques which usually combine contact excitation methods with noncontact detection methods[36, 14]. Laser interferometry has wide use in signal detection of ultrasonics. Another application of laser ultrasonics is the excitation by continuous and pulsed lasers. The advantage of these methods are in the almost unrestricted field for an application and the noncontact character which has advantages over conventional contact techniques[81, 21, 74]. White demonstrated first experiments with radiation generated ultrasound[87]. Further development of

laser apertures [63, 74] made the laser a useful device for ultrasonic excitation. For nonlinear ultrasonics, the broadband signal by a laser pulse[20] can be manipulated to a narrowband harmonic source by spatial arrays[72]. Approaches for the patterning of the laser beam were made by the use of a lens array[20, 55], multiple laser beams and interference[57, 33, 62, 59, 61], a diffraction grating [40] and a shadow mask[23, 70, 9, 60]. The last technique was used by [60] to characterize the nonlinearity of fatigue damage on an aluminum alloy. Those references are executed with an excitation source beyond the threshold of the materials surface and it is desirable in the field of nondestructive evaluation[8] to not damage the surface of the specimen. However the thermoelastic regime is known for its signals with low amplitude and signal to noise ratio[30]. Increasing the incident laser pulse energy results in higher amplitudes [51, 56, 43, 58] but also damages the surface due to the ablation of thin material layers[48]. For an analytical description, Scruby et al. (1980)[73] treated the thermoelastic source as an expanding point volume resulting in orthogonal force dipoles and Rose (1984)[68] developed the mathematical basics by integral transforms for a point source by his surface center of expansion theory (SCOE). A complete model for near and farfield of the thermoelastic source was made by Spicer (1990)[79] and Achenbach (2003)[4] developed a model for the excited wave field by thermoelastic line and point sources without the use of integral transforms. The modulation of the source in the ablative regime is more difficult due to uncertainties in the exciting mechanisms. The source is represented as an equivalent mechanical force normal to the specimens surface excited by the linear momentum of repelled material[58, 74, 48].

1.3 Content and Structure of the Thesis

This thesis contains the following outline. Chapter 2 gives an brief introduction into the phenomena and characteristics of ultrasonics and provides the basic theory

for nonlinear wave propagation. Chapter 3 is an introduction into laser ultrasonics. The focus in this chapter is on the characterization of the excitation of ultrasound by thermoelastic and ablative sources and a mathematical model for an analytical solution of the thermal excited elastic wave problem is presented. The experimental set ups are introduced in Chapter 4 including measurement procedures and the signal processing. The characterization of the laser excited acoustic source and the results for its application for the detection of material nonlinearities is presented and discussed in Chapter 5. A final discussion of the developed technique follows in Chapter 6 including a review of the experiments and the results as well as recommendations for improvements and future work.

CHAPTER II

INTRODUCTION INTO WAVEPROPAGATION

For nondestructive evaluation different wave phenomena are used to investigate structures for flaws and materials for their properties. In this chapter basics of linear and nonlinear wave propagation are provided by introducing principles of acoustic waves. The introduction discusses only bulk and surface waves due to the focus of the experimental procedures.

2.1 Wave Phenomena

2.1.1 Equation of Motion

A body shall be defined by its volume V and surface area A_V . The general equation of motion for the continuum is derived by the balance of linear momentum:

$$\int_A \mathbf{t} dA_V + \int_V \rho \mathbf{f} dV = \int_V \rho \ddot{\mathbf{u}} dV \quad (2.1)$$

The traction \mathbf{t} is the force per unit area dA defined by the normal vector \mathbf{n} (Fig. 2.1), ρ is the mass density, \mathbf{f} the body force and \mathbf{u} is the particle displacement. The components of the traction vector t_i are derived by the stress tensor τ by

$$t_j = \tau_{ji} n_i \quad (2.2)$$

where τ is a symmetric tensor of second order for a nonpolar elastic medium[52]. Using the Gauss's Divergence theorem (Eq. A.1) and Eq. 2.2 the balance of linear momentum is written as a volume integral in index notation of the form

$$\int_V \tau_{ji,i} + \rho f_j - \rho \ddot{u}_j dV = 0 \quad (2.3)$$

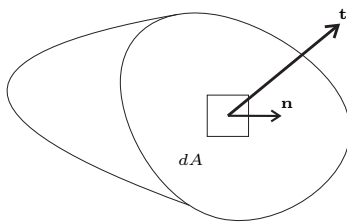


Figure 2.1: Traction force acting on a unit area with normal vector \mathbf{n}

and the equation of motion is derived as

$$\tau_{ij,i} + \rho f_j = \rho \ddot{u}_j. \quad (2.4)$$

In the following we want to express Eq. 2.4 only in terms of displacement and derive a description for a propagating disturbance in a solid. The stress strain relationship is expressed by the fourth order tensor \mathbf{C} :

$$\tau_{ij} = C_{ijkl} \epsilon_{kl} \quad (2.5)$$

with the components ϵ_{kl} of the strain tensor, ϵ and \mathbf{C} can be expressed for a homogeneous, isotropic, elastic medium by

$$C_{ijkl} = \lambda \delta_{ij} \delta_{kl} + \mu (\delta_{ik} \delta_{jl} + \delta_{il} \delta_{jk}) \quad (2.6)$$

with the Kronecker-Delta δ_{ij} (Eq. A.2) and the Lamé-constants denoted by λ and μ and Hooke's law

$$\tau_{ij} = \lambda \epsilon_{kk} \delta_{ij} + 2\mu \epsilon_{ij} \quad (2.7)$$

is derived and we are able to replace the stresses by strain relations in Eq. 2.4. Finally by applying the relationship

$$\epsilon_{ij} = \frac{1}{2} (u_{i,j} + u_{j,i} + u_{i,j} u_{j,i}), \quad (2.8)$$

where the last term can be neglected for the linear case, provides Navier's equation of motion in terms of displacements:

$$\mu u_{i,jj} + (\lambda + \mu)u_{j,ji} + \rho f_i = \rho \ddot{u}_i \quad (2.9)$$

This is a partial differential equation. In order to decouple the equation the Helmholtz decomposition is used, where the state of the continuum is described by scalar a scalar potential φ and a vector potential ψ .

$$\mathbf{u} = \nabla\varphi + \nabla \otimes \psi \quad (2.10)$$

where \otimes denotes the vector product, using a constraint condition that the vector potential is divergence free, $\nabla\psi = 0$. Using Eq. 2.9 and Eq. 2.10 two uncoupled differential equations are derived:

$$\nabla^2\varphi = \frac{1}{c_L^2}\ddot{\varphi} \quad (2.11)$$

$$\nabla^2\psi = \frac{1}{c_S^2}\ddot{\psi} \quad (2.12)$$

Here c_L and c_S are the velocities of the longitudinal and the transversal wave-field respectively. These are material properties and can be described in terms of Lamé-constants and the density:

$$c_L = \sqrt{\frac{\lambda + 2\mu}{\rho}}, \quad c_S = \sqrt{\frac{\mu}{\rho}} \quad (2.13)$$

Here $c_L > c_S$ always holds[2].

2.1.2 Plane Waves

For theoretical analysis of wave problems it is useful to assume plane wave properties for a propagating wave. This means that the properties such as stress and strain of

the disturbance with a propagation speed c in direction \mathbf{p} are constant in any plane orthogonal to the propagation direction \mathbf{d} .

$$\mathbf{u} = \mathbf{d}f(\mathbf{p} \cdot \mathbf{x} - ct) \quad (2.14)$$

with $|\mathbf{d}| = 1$ describing the direction of particle motion and an arbitrary real function $f(\mathbf{x}, t)$ describing the shape of the disturbance. Substitute 2.14 into the Navier equation of motion (Eq. 2.9) results in

$$(\mu - \rho c^2)\mathbf{d} + (\lambda + \mu)(\mathbf{p} \cdot \mathbf{d})\mathbf{p} \quad (2.15)$$

with solutions only for

$$\mathbf{d} = \pm\mathbf{p}, \quad (2.16)$$

particle movement in same direction same as propagation direction, longitudinal waves, or

$$\mathbf{d} \cdot \mathbf{p} = 0 \quad (2.17)$$

particle movement is perpendicular to propagation direction, shear/transversal waves.

2.2 Bulk and Surface Waves

Harmonic representation of wave fields in space and time are useful in many cases, such as nonlinear ultrasonics. A harmonic wave with particle motion in the $x_1 - x_2$ directions can be described as

$$\mathbf{u} = A\mathbf{d}e^{ik(x_1p_1+x_2p_2-ct)} \quad (2.18)$$

where A is the amplitude, p_1, p_2 are the components of the propagation vector. The wave number, k , is defined as

$$k_L = \frac{\omega}{c_L} \quad (2.19)$$

for longitudinal waveforms and

$$k_S = \frac{\omega}{c_S} \quad (2.20)$$

for transversal waves and circular frequency ω .

The interaction of a wave form like in Eq. 2.18 with a free boundary ($\tau_{ij,j}n_j$) an incident plane wave is reflected. The wave field that results depends on the angle between the propagation vector \mathbf{d} and the surface normal (Fig. 2.2). A incident longitudinal wave field with incident angle θ_0 (Fig. 2.2 a)) will be reflected as a superposition of reflected longitudinal wave field (P), reflected in an angle θ_1 and a transversal shear wave field (SV) with particle motion in the $x_1 - x_2$ plane and reflection angle θ_2 . Phase matching of the incident and reflected wave fields, the so called Snell's law, results in the condition

$$k_0 \sin \theta_0 = k_1 \sin \theta_1 = k_2 \sin \theta_2. \quad (2.21)$$

The same holds for an incident transversally polarized shear wave (Fig. 2.2 b)). Special cases are for an incident angle $\theta_0 = 0$ when the incident wave is reflected normally as itself. If the incident angle is smaller than the materials critical angle $\theta_r = \arcsin(c_S/c_L)$ the reflected longitudinal wave propagates in the x_1 -direction and decays exponentially with depth into the half-space[2].

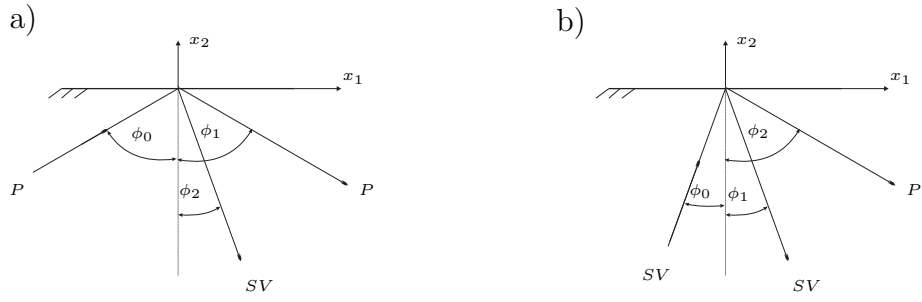


Figure 2.2: Incident and reflected wave field for longitudinal (P)- and transversal (SV) waves in a unbounded half-space

2.2.1 Rayleigh Waves

The derivations in the above results in the generation of Rayleigh surface waves. The potential functions for the 2-D case are

$$\varphi = C_1 e^{-k_R q x_2} e^{i k_R (x_1 - c_R t)}, \quad x_2 \leq 0 \quad (2.22)$$

and

$$\psi = C_2 e^{-k_R h x_2} e^{i k_R (x_1 - c_R t)} \quad x_2 \leq 0. \quad (2.23)$$

With the constants $q = \sqrt{1 - \left(\frac{c_R}{c_L}\right)^2}$, $h = \sqrt{1 - \left(\frac{c_R}{c_S}\right)^2}$ and arbitrary C_1 and C_2 . The Rayleigh wave number is $k_R = \omega/c_R$ with the characteristic Rayleigh wave speed c_R which is about 90% of the shear wave speed [85]. The solution of the wave equations 2.11 and 2.12 for the vector potentials of the Rayleigh wave yields

$$\left(2 - \frac{c_R^2}{c_S^2}\right)^2 - 4\sqrt{\left(1 - \frac{c_R^2}{c_L^2}\right)\left(1 - \frac{c_R^2}{c_S^2}\right)} = 0 \quad (2.24)$$

and has no frequency, ω , dependence. Thus the solution for the phase velocity is nondispersive. In a good approximation

$$c_R = \frac{0.862 + 1.14\nu}{1 + \nu} \quad (2.25)$$

where ν is the Poisson's ratio[2].

The wave field of the Rayleigh wave is a combination of longitudinal and transversal

displacements. Due to a phase shift of $\pi/2$ between the displacements in x_1 and x_2 and a vertical displacement that is typically about 1.5 times the horizontal displacement the Rayleigh wave has an elliptical particle motion counter clockwise when propagating in positive x_1 direction[31] (Fig. 2.3).

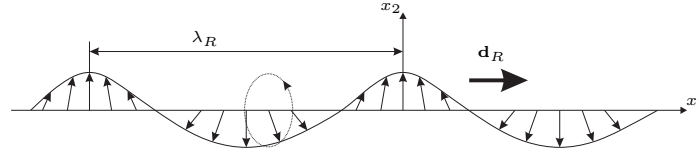


Figure 2.3: Rayleigh surface wave schematic

The wave field decays exponentially in negative x_2 -direction and in a depth of about $0.192 \times \lambda$ the elliptical particle motion changes the direction. The benefit of the dispersion free propagating Rayleigh wave is that the energy of the wave is located in the surface layers of the the material and thus the wave propagates long distances without significant losses and is suitable for the nondestructive evaluation of surface layers and the detection of surface flaws.

2.3 Nonlinear Wave Theory

The derivations and solution of the wave equation above assume linear behavior of the propagating wave. This assumption is quite sufficient in many NDT applications for the detection of macro flaws and damages. However, it might be of value in the field to detect damage before it occurs and may lead to the defect of a structure. Damages like fatigue damage, creep or damage due to corrosion originate due to changes of the materials micro structure and dislocations(Fig. 2.4).

In linear continua, a harmonic signal launched into the material will be detected as a signal with the same frequency content. In nonlinear continua micro structure

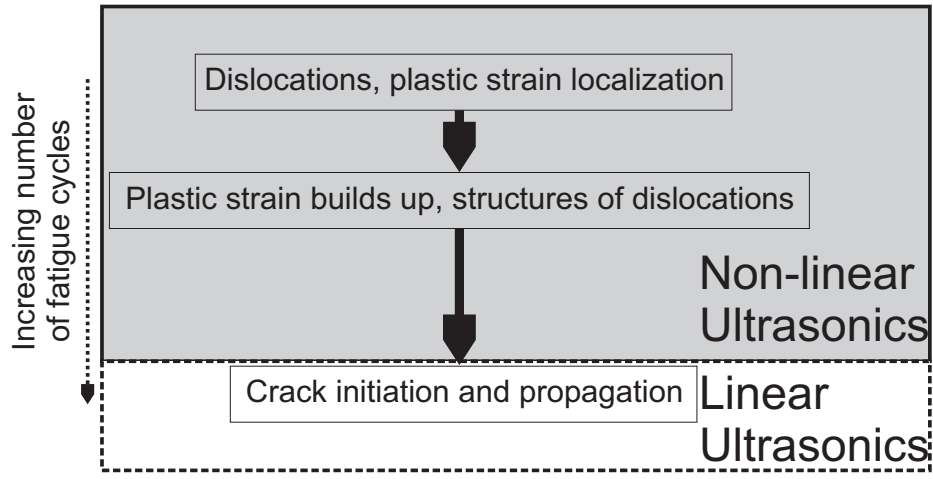


Figure 2.4: Fatigue damage and acoustic detection

damage as well as micro cracks provide an excitation of higher harmonics of the original signal like in the schematic of Fig. 2.5.

$$U_{in} = A_{in}(\omega, t, \mathbf{x}) \begin{array}{l} \xrightarrow{\text{Linear Continuum}} U_{out} = A_{out}(\omega, t, \mathbf{x}) \\ \xrightarrow{\text{Non-linear Continuum}} U_{out} = A_1(\omega, t, \mathbf{x}) + A_2(2\omega, t, \mathbf{x}) + \dots \end{array}$$

Figure 2.5: Higher harmonic excitation in nonlinear continua.

2.3.1 Nonlinear Wave Equation

While the linear wave propagation assumes a linear stress-strain relationship, nonlinear ultrasonics applies a nonlinear stress-strain relationship. Assuming nonlinear strain behavior (Eq. 2.8) and neglecting constant stresses, the nonlinear stress-strain relationship is written as

$$\tau_{ij} = C_{ijkl}\epsilon_{kl} + \underbrace{C_{ijklmn}}_{3^{rd}\text{-order elastic constants}} \epsilon_{kl}\epsilon_{mn} + \dots \quad (2.26)$$

with τ in current configuration \mathbf{x} (Fig. 2.6) and the assumption of a weakly nonlinear material[88], where the nonlinearity of the material dominates nonlinearities of the geometry.

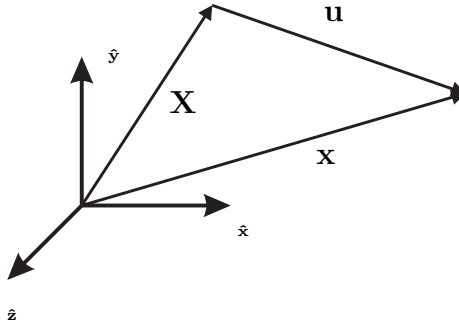


Figure 2.6: Schematic of current and reference configuration

As the relationship is nonlinear, the Piola-Kirchoff stress \mathbf{P} in terms of the reference configuration (Eulerian coordinates) has to be used to determine the stresses in the material/current configurations in Lagrangian coordinates[52]

$$\sigma = \frac{\rho}{\rho_0} \mathbf{P} \mathbf{F}^T \quad (2.27)$$

with the density ρ and ρ_0 in the current and the reference configuration respectively and the deformation gradient, $\mathbf{F} = \frac{\partial \mathbf{x}}{\partial \mathbf{X}}$. The equation for the linear momentum is

$$\rho_0 \ddot{\mathbf{u}} = \nabla_{\mathbf{x}} \mathbf{P}. \quad (2.28)$$

In the next step the \mathbf{P} is related to the Lagrangian strain tensor with components according to Eq. 2.8 with the derivatives with respect to the Eulerian coordinates[32]:

$$P_{ij} = \rho_0 \frac{\partial W}{\partial F_{ij}} \quad (2.29)$$

with the strain energy by unit mass, W . Using Eq. 2.26 and the momentum equation, the nonlinear wave equation is derived as

$$\rho_0 \frac{\partial^2 u_i}{\partial t^2} = \frac{\partial^2 u_k}{\partial X_j \partial X_l} \left(C_{ijkl} + M_{ijklmn} \frac{\partial u_m}{\partial X_n} + \dots \right) \quad (2.30)$$

where

$$M_{ijklmn} = C_{ijklmn} + C_{ijln}\delta_{km} + C_{jnkl}\delta_{im} + C_{jlmn}\delta_{ik}. \quad (2.31)$$

2.3.1.1 Materials Nonlinearity

In the one dimensional case for longitudinal waves, the wave equation reduces to

$$\frac{\partial^2 u}{\partial t^2} = c_L \frac{\partial^2 u}{\partial X^2} \left[1 - \beta \frac{\partial u}{\partial X} \right] \quad (2.32)$$

with the nonlinearity parameter

$$\beta = - \left(\frac{3}{2} + \frac{C_{111}}{2\rho_0 c_L^2} \right). \quad (2.33)$$

The solution to Eq. 2.32:

$$U_{out} = A_1 \sin(\omega t - kx) + \underbrace{\frac{\beta}{8} \left(\frac{\omega A_1}{c_L} \right)^2}_{A_2} x \sin(2\omega t - 2kx) \quad (2.34)$$

In Eq. 2.34 it can be seen, that the amplitude of the second harmonic wave increases with the propagated distance x and with the nonlinearity parameter β and scales with the square of the first harmonic amplitude $A_2 \propto A_1^2$. Using the amplitudes of the first and second harmonic, the nonlinearity parameter β is

$$\beta = \frac{8c_L^2}{\omega^2 x} \frac{A_2}{A_1^2}. \quad (2.35)$$

Knowing the wave velocity and the excited frequency, β can be determined by measuring A_1 and A_2 .

Nonlinearity of Rayleigh Waves For the nonlinearity of Rayleigh waves it shall be noted that for isotropic materials the shear wave does not develop a nonlinearity due to the symmetry of the third order elastic constants. Thus it can be assumed that the nonlinearity coefficient of the Rayleigh wave, since Rayleigh waves

are the superposition of longitudinal and shear waves propagating in with c_R , also scales with the ratio A_2/A_1^2 . Herrmann et al. (2005) derived β for Rayleigh waves[36]. The equations 2.22 and 2.23 are rewritten as

$$\varphi = -i \frac{B_1}{k_R} e^{px_2} e^{i(k_R x_1 - \omega t)} \quad (2.36)$$

and

$$\psi = -i \frac{D_1}{k_R} e^{sx_2} e^{i(k_R x_1 - \omega t)} \quad (2.37)$$

where $p^2 = k_R^2 - k_L^2$ and $s^2 = k_R^2 - k_S^2$. For the stress free boundary condition the constants B_1 and D_1 are related by

$$B_1 = -i \frac{2k_R p}{k_R^2 + s^2} D_1. \quad (2.38)$$

The displacement field of the Rayleigh wave is decomposed into an out-of-plane

$$u_{x_1} = B_1 \left(e^{px_2} - \frac{2ps}{k_R^2 + s^2} e^{sx_2} \right) e^{i(k_R x - \omega t)} \quad (2.39)$$

and in-plane component

$$u_{x_2} = -i B_1 \frac{p}{k_R} \left(e^{px_2} - \frac{2ps}{k_R^2 + s^2} e^{sx_2} \right) e^{i(k_R x - \omega t)}. \quad (2.40)$$

and the generated second harmonic waves due to the materials nonlinearity is also decomposed in a similar way, i.e a out-of-plane component

$$u_{x_1} = B_2 \left(e^{2px_2} - \frac{2ps}{k_R^2 + s^2} e^{2sx_2} \right) e^{i2(k_R x - \omega t)} \quad (2.41)$$

and in-plane component

$$u_{x_2} = -i B_2 \frac{p}{k_R} \left(e^{2px_2} - \frac{2ps}{k_R^2 + s^2} e^{2sx_2} \right) e^{i2(k_R x - \omega t)}. \quad (2.42)$$

Considering that only the longitudinal components are subject to the nonlinearity in the material, equations 2.39 and 2.41 can be related in the same fashion as above for 1-D longitudinal wave fields as

$$B_2 = \frac{\beta k_L^2 x B_1^2}{8}. \quad (2.43)$$

For the detection of the nonlinearity of surface waves the common detection equipments (Section 4.5) and specially noncontact methods like laser-interferometer are predominantly sensitive for the out of place displacement of the surface. Using the assumptions above and the surface displacements $u_{x_2}(\omega, t, x_1, x_2 = 0)$ the nonlinear parameter results in

$$\beta = \frac{u_{x_2}(2\omega)}{u_{x_2}^2(\omega)} \frac{8ip}{x k_L^2 k_R} \left(1 - \frac{2k_R^2}{k_R^2 + s^2} \right). \quad (2.44)$$

CHAPTER III

LASER ULTRASONICS

Lasers can be used for generation and detection of ultrasound. Laser detection methods like the Michelson interferometer are well known measurement procedures for vibrations and acoustic waves. Laser generation methods were first applied by White[87] in the 1960s. Nowadays the excitation is by pulsed lasers in the thermoelastic and ablative regime. The application of laser excitation methods in research and industry has increased in the last two decades[64]. However huge costs and the size of the equipment restrict an increase in use.

A common method used for launching and detection of an acoustic signal in a solid is the contact transducer technique. Common contact transducers are piezoelectric transducers which are based on the ceramic PZT (lead zirconate titanate). A contact transducer is attached to the surface of the specimen, usually done by coupling it to a medium like water or oil to transmit the acoustic signal into the specimen. The mechanical characteristics of the transducer, the necessity of full-time contact, and the use of a coupling medium causes several drawbacks within this way of excitation and detection procedures.[81] Contact methods suffer from influences introduced by the coupled surfaces and the coupling medium[72]. While the use of insufficient amounts of couplant result in dry areas between the coupled surfaces and thus, in an inadequate contact, the use of excessive amounts of couplant can result in losses and the development of resonances of the signal in the coupling medium with negative influences on the excited and the detected signal. Further disadvantages of contact transducers are slow scanning speeds when a large area needs to be examined and the load of the attached transducer on the surface[74]. Also the use of piezoelectric

transducers and a coupling medium may not be possible in some circumstances or systems such as high temperatures, high radioactivity, hazardous atmospheres, narrow spaces, dynamic systems and materials that are sensitive to corrosion when they are in contact with the coupling medium[74, 81, 43, 64]. Therefore non-contact excitation and detection principles are highly interesting for non-destructive evaluation in these circumstances and systems.

3.1 Non-contact Methods

Several non-contact ultrasonic methods have been developed as alternatives to contact transducers compensating most of their disadvantages. Common non-contact methods are, e.g. the use of EMATS (electromagnetic acoustic transducers), capacitive transducers, air coupled transducers, optical excitation and detection methods, etc. The use of optical methods like laser generation and detection reduce several shortcomings of contact and other non-contact systems. Advantages of laser generation methods compared to other non-contact methods are the adaptability of the excitation method to the specimen's material, the shape and the investigated material property or damage by variation of laser settings like pulse width, energy and geometry of the illuminated surface area.[38]

In this thesis a laser excitation method is investigated and developed. As the laser detection is not used in this thesis, the method will not be described any further. With respect to the principles and applications of interferometry please see the references [74, 80, 34].

3.2 Laser Generation Methods

Laser-irradiation methods to excite acoustical pulses were first described by White (1962) who excited acoustic waves using the effect of the materials thermoelastic expansion caused by electron bombardment and the absorption of electromagnetic energy[87]. Later Ledbetter et al. discovered that laser penetration of a surface

elastic excites longitudinal, transverse and Rayleigh surface waves[49].

The thermoelastic generation of ultrasound was primarily used to detect flaws and measure material constants. The broadband frequency spectrum of a laser source can extend up to 100 *MHz* and is inversely proportional to the laser pulse width[20]. As long as the incident pulse energy is beyond a certain level around 100 *MW/cm²* for metals like aluminum and steel [27] where no plasma is formed[6] and the thermal expansion of the material acts as an elastic wave source. Above this threshold intensity the surface material melts and vaporizes. A visible damage is left on the surface. According to the resulting surface damage, it is arguable if the laser ultrasonic in the ablative regime is a truly non-destructive evaluation technique. Such a technique should be applied in a field of more robust structures[43].

3.2.1 Laser

The laser might be one of the most important scientific and technical achievements of the last century, beginning by Albert Einstein and the process of stimulated emission and the quantum theory. However it was in the 1960s when the first laser working in optical frequencies was developed[63]. Shortly afterwards White used radiation sources to excite ultrasound in solids[87]. While mainly pulsed lasers are used for ultrasonic excitation, continuous lasers are mainly applied in the signal detection. This development of the laser quickly overtook conventional optical measurement methods[74] like the Schlieren photography.

A laser is a device that emits electromagnetic radiation with a frequency spectrum of between less than 10^4 *Hz* (long radio waves) and 10^{21} *Hz* (high energy gamma waves), and a propagation velocity of $c = 2.9979 \times 10^8$ *ms⁻¹*. The invention of the laser made it possible to generate strictly monochromatic electromagnetic radiation in the wavelength range of 200 *nm* to 10 μ *m*, which was not possible before and can

be used in the field of ultrasonic excitation and detection.

In electromagnetic radiation, energy is periodically transferred between electric and magnetic energy. The electric and magnetic fields are perpendicular to each other in a plane normal to the direction of propagation of the electromagnetic wave. The orientation of the electric and magnetic field can result in the polarization of the radiation[63]. If the orientation of the field is constant, the radiation is called in-plane polarized. In the case of a rotating electric (and magnetic) field of constant amplitude, the radiation is called circularly polarized. In general, superposition of both principles leads to the elliptical polarization[74] of polarized light. The polarization of the emitted laser light is of higher importance in the detection than in the generation of ultrasound, which is more dependent on the total laser energy and pulse width.

The following description gives a brief introduction into the principles of the generation of efficient laser light. According to the quantum theory light behaves like a collection of small discrete particles, called photons. The energy of a photon is defined as $h\nu^r$, with the Planck's constant h and the frequency of the radiation, ν^r . The energy states of atomic and molecular systems are described by discrete energies such as the ground state E_0 and multiple excited states E_n . Absorption of energy can excite an energetic system (like an atom) to a higher energy level. The energetic system can then return to a state of lower energy by the emission of radiation. The absorption and emission process is quantized by the energy difference of energetic levels. To excite a system from the E_0 state to the E_1 state 3.1 the absorption of electromagnetic radiation with a frequency ν^r is needed, such that

$$h\nu^r = E_1 - E_0. \tag{3.1}$$

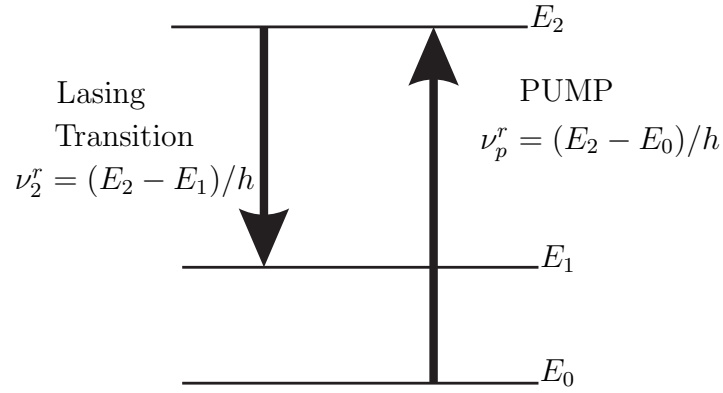


Figure 3.1: Discrete energy level diagram for the stimulation principle.

In the same manner radiation is emitted during a decrease energy of a higher to a lower energy level. This emission can occur spontaneously or due to a process called stimulated emission. Here external penetration, e.g. radiation with the same wavelength, causes the system to emit radiation. This process is used by LASERS (Light Amplification by Stimulated Emission Radiation) to excite a laser medium that emits radiation in the desired wave length. A model system consists of matter with three energy levels $E_0 < E_1 < E_2$ [74] (a real system can have more than three energy levels). According to the Boltzmann distribution the number of particles N_i having a certain energy level is

$$N_i = N_0 e^{-(E_i/k^B T)} \quad (3.2)$$

here k^B is the Boltzmann constant and T is the absolute temperature of the system in Kelvin. When the atoms absorb radiation in the form of

$$h\nu_p^r = E_2 - E_0 \quad (3.3)$$

they get excited into the higher state E_2 by absorbing the so-called pump frequency ν_p^r . Due to pumping, the populations of E_0 and E_2 tend to equalize, leading to an effect called population inversion between the E_1 and E_2 levels. The whole system

will try to correct this inverted state by the emission of energy

$$h\nu_r = E_2 - E_1 \quad (3.4)$$

where $\nu_p^r > \nu^r$. For this process a laser needs both a source for the stimulated emission and a source for a technical efficient generation, meaning the possibility to feed emitted radiation back into the system in order to build up a sustained oscillation of emission. Pumping can be done in two ways. Either an intense light source is used to illuminate the medium, or voltage is applied to discharge the laser gas. In order to achieve a sustainable oscillation for a sufficiently strong and constant laser source, the radiation is led back into the system. This is realized by a resonant system, e.g. by high performance mirrors (Fig. 3.2). For each pass the radiation takes more emission is stimulated and the intensity of the radiation is amplified, which is known as a resonant cavity[74]. To allow the external use of the emitted radiation of the system an outlet is necessary. Often one of the mirrors has the property to allow a small fraction of the incident radiation to be transmitted.

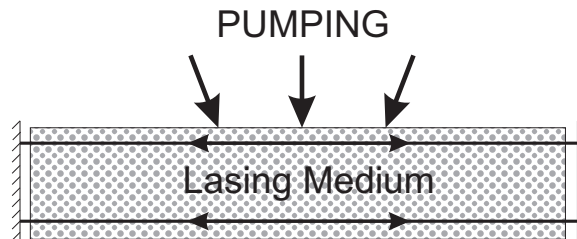


Figure 3.2: Basics of the laser oscillator

Lasers using this principle are able to emit radiation with a pulse width of $0.1 \text{ ms} - 1 \text{ ms}$. For the generation of ultrasound an additional technique is required to obtain the desired pulse lengths of $1 \mu\text{s}$ to $100 \mu\text{s}$. The Q-factor is the ratio between the energy stored in the oscillator and the energy lost by the cavity per round trip. A low Q suppresses the cavity oscillations and the population inversion can be increased

above the usual threshold. Changing the Q from low to high levels results in a rapid emission of the desired photons which allows a short laser pulse to be emitted from the aperture[31].

3.2.2 Absorption of Electromagnetic Radiation

Laser illumination of the surface of a solid can cause different physical processes primarily depending on the power density of incident laser beam which is in charge for the ultrasonic generation. At a low power density, the material is locally heated and both thermal and elastic waves are generated. In semiconductors also electric currents may develop. At higher power densities material ablation takes place and a plasma is formed. The surface material melts, vaporizes and deforms plastically. In the worst case this initiates the formation of cracks[74].

The amount of energy absorbed by the target material of an incident laser pulse mainly depends on the optical material properties and the surface quality. Assuming sufficient thickness of a material which is opaque for the laser light, one part of the energy is absorbed by various mechanisms which mainly depend on material characteristics and the wavelength of the laser pulse[74] while the other part is reflected. Using a non-reflective surface with the assumption that plane waves move into the material like in Fig. 3.3 while the absorption takes place in the so called skin depth of the material and the thermal wave field is in the range of a few micrometers for Q-switched lasers. In a regime in which no plasma shielding occurs, the absorbed intensity δI is

$$\delta I = \gamma I \delta z \tag{3.5}$$

with the thickness δz of the absorbing infinitesimal element and the absorption coefficient γ . By integration the exponential form of absorption results in

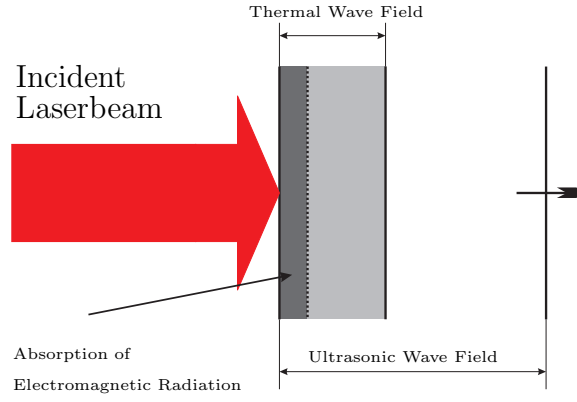


Figure 3.3: Absorption of electromagnetic radiation and the resulting thermal and acoustic wave field[72]

$$I = I(0)e^{-\gamma z}. \quad (3.6)$$

For a material with reflecting surface, the reflectivity is defined as

$$R = I''/I \quad (3.7)$$

with the reflected intensity

$$I'' = I - I' \quad (3.8)$$

and the absorbed intensity I . The absorption of the electromagnetic radiation takes place on the surface layer of the material, the skin depth (Fig. 3.3). The skin depth is defined as the depth δ for which a wave's amplitude decays by $1/e$ of its original amplitude. For a longer wavelength like in the infra red regime the skin depth can be calculated to

$$\delta = (\pi\sigma\mu_r\mu_0\nu^r)^{-1/2} \quad (3.9)$$

with the conductivity σ , the relative permeability μ_r , and the permeability $\mu_0 = 4\pi * 10^{-7} Hm^{-1}$ [15]. The formula is restricted to lower frequencies, such as present

in the infra red (IR) regime. For higher frequencies quantum mechanic aspects have to be considered. For $\sigma = 4 * 10^7 (\Omega m)^{-1}$ and the value $\mu_r \approx 1$ for aluminum and a radiation of $1.06 \mu m$ the skin depth results in $5 nm$. The skin depth can be used to calculate the reflectivity on a clean surface as

$$R = \frac{2 - 2\xi + \xi^2}{2 + 2\xi + \xi^2} \quad (3.10)$$

with $\xi = \mu_0 \sigma \mu_r c \delta$, and c the velocity of light. However, for most metals and low optical frequencies it follows $\xi \gg 1$ and

$$R = 1 - 4/(\mu_0 \sigma c \delta) \quad (3.11)$$

resulting in a reflectivity of 0.94 for polished aluminum. For the ablative regime the physical procedures are getting much more complicated. When the optical power increases about the threshold for ablation, surface material is molten and vaporizes. The vapor is ionized and a plasma is formed [27] which shields the surface of the incident laser beam [48] partially or in total.

3.2.3 Temperature Distribution

Especially for laser excitation in the thermoelastic regime the temporal and spatial distribution of the temperature T of the material is of interest, as it directly results in a thermal expansion of the material and thus in a thermoelastic excited wave. For low laser power, a uniformly illuminated area A , and an extremely short pulse width, it was first assumed that the thermal conductivity could be neglected. The assumption of a uniform absorption on the skin depth induces a temperature increase on the surface of

$$\delta T = \delta E / C \rho A \delta \quad (3.12)$$

with the absorbed pulse energy δE , the specific heat capacity C and the density ρ . For the values of polished aluminum and an irradiated area of 10 mm^2 by an 100 mJ pulse, this would result in a temperature increase of about 5000 K and thus a vaporization of the surface layer. This result does not confirm the assumption of no influence of the conductivity at these intensities[73]. In fact, laser pulses with a width in the range of $10 - 100 \text{ ns}$ penetrate material to a depth of about $1 \text{ }\mu\text{m}$ and the value of the temperature increase of 5000 K is reduced to a value of 100 K according to Eq. 3.12 which is more reasonable.

A more accurate temperature distribution is derived from the differential equation of heat flow in a semi infinite half-space with a boundary at the plane $z = 0$:

$$\Delta^2 T - \frac{1}{\kappa} \frac{\partial T}{\partial t} = -\frac{A_V}{K} \quad (3.13)$$

with thermal conductivity K , thermal diffusivity κ , and the heat produced per volume area $A_V(x, y, z, t)$. Using the boundary conditions $T(x, y, z, 0) = 0$ and $T \rightarrow 0$ for $z \rightarrow \infty$ and no heat flux at $z = 0$.

In the most cases the three dimensional problem can be reduced to a one dimensional problem, as the irradiated surface of the material is much larger compared to the depth to which the heat is conducted [74]:

$$T = T(z, t); A_V = A_V(z, t) \quad (3.14)$$

Solving this differential equation[16],it is

$$T(z, t) = \frac{2I'(\kappa t)^{1/2}}{K} \text{ierfc} \left(\frac{z}{2(\kappa t)^{1/2}} \right) \quad (3.15)$$

with

$$ierfc(\zeta) = \frac{1}{\sqrt{\pi}}e^{-\zeta^2} - \frac{2\zeta}{\sqrt{\pi}} \int_{\zeta}^{\infty} e^{-\xi^2} d\xi. \quad (3.16)$$

For a pulse switched on at $t = 0$ and switched off at $t = t_0$ a second term must be added and the temperature distribution is:

$$T(z, t) = \frac{2I'(\kappa t)^{1/2}}{K}ierfc\left(\frac{z}{2(\kappa t)^{1/2}}\right) - \frac{2I'(\kappa(t-t_0))^{1/2}}{K}ierfc\left(\frac{z}{2(\kappa(t-t_0))^{1/2}}\right) \quad (3.17)$$

As a result the temperature distribution for short duration scales (~ 75 ns) on the material's surface mainly depends on the pulse width and the peak energy (for non uniform profiles) while for longer durations (~ 150 ns) and deeper conduction distances the total energy is most relevant. A spatial and temporal pulse of Gaussian shape results in more moderate temperature maxima and gradients, specially for short pulse widths[74].

3.2.4 Thermoelastic and Ablative Heat Source

Depending on the pulse energy of an incident laser beam at a solid surface, acoustic bulk shear and surface waves (where the most significant part of the signal propagates with the velocity of Rayleigh surface Waves[5]) are generated. According to the previous sections, working at low energies results in a thermoelastic expansion of infinitesimal surface volumes[74, 4] and the resulting tangential forces[72] work as the acoustic source. At high energies ablation of the surface material occurs and the acoustic source is due to a strong normal force generated by the ablation processes. Fig. 3.4 shows the radiation pattern for a thermoelastic and an ablative point source. For the ablative regime, most of the pressure pulse energy goes forward into the material[27].

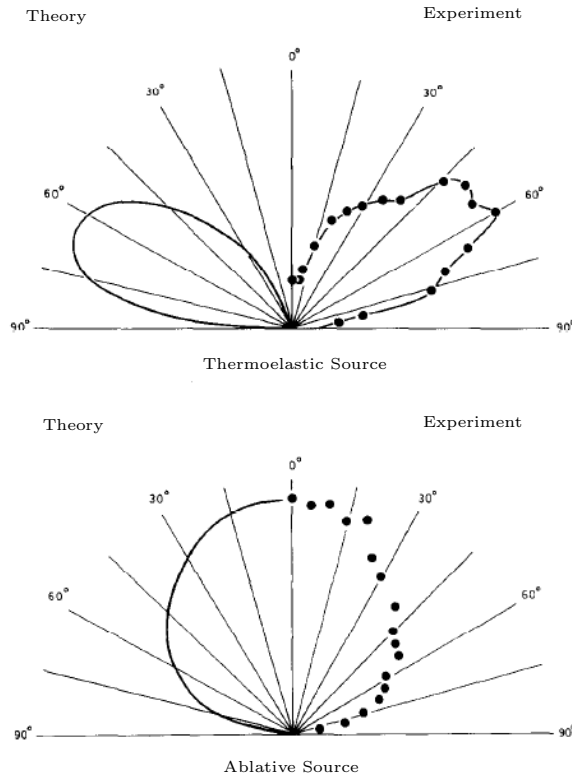


Figure 3.4: Farfield pattern of compression wave by laser pulse[72]

The different generation principles cause different characteristics in the excited wave field. Depending on the applied energy in the ablative regime, the acoustic source is a superposition of a thermoelastical and an ablative source[58, 27], where the normal force mechanism becomes more dominating with an increasing laser power density.

Thermoelastic excited waves are suitable to generate well defined narrowband signals [72, 40] with a waveform that is independent of the pulse energy[38] and a magnitude scaling[87, 6, 27, 69, 22] with the incident pulse energy. Relatively small amplitude[30] can be expected and a small signal to noise ratio[8], compared to ablative excitation mechanisms[51]. Increasing the laser power above the threshold of ablation increases the magnitude of the resulting waveforms noticeably[58, 56, 43] especially for longitudinal and surface waves[22] (see Fig. 3.5):

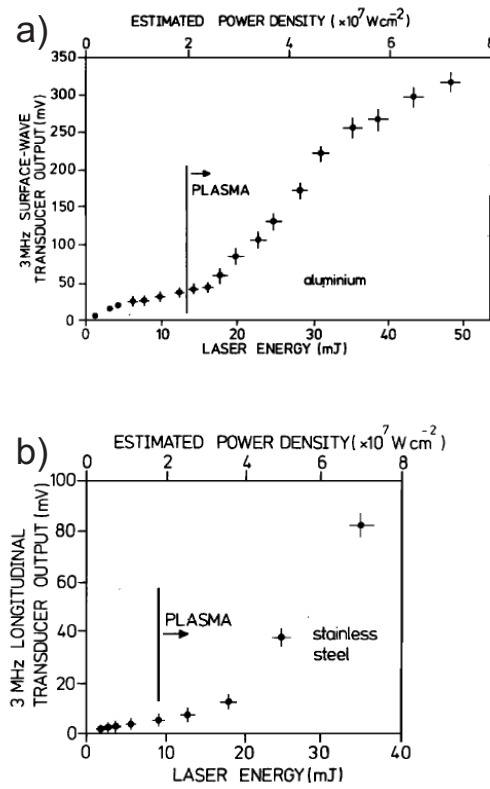


Figure 3.5: Signal Amplitude of a) longitudinal wave, b) Rayleigh surface wave in aluminum as a function of incident pulse energy[6]

While the thermoelastic source tends to excite high amplitudes for transversal waves[6], the excitation in the ablative regime decreases with incident energy and vanishes completely[22] when large plasmas are generated(Fig. 3.6).

When the laser power is above the threshold of the material, the irradiated surface is first heated up to the melting temperature of the material. The melt front is propagating into the material and for continuous heating the material will start to vaporize. Specially for ablation with lower pulse energies, e.g. use of lasers that are not Q-switched, the thermal conductivity of the material determines the amount of material being vaporized[67]. A thin layer on the surface, the Knutsen-layer, is formed

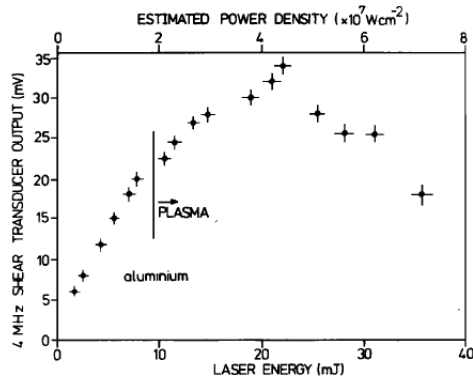


Figure 3.6: Signal Amplitude transversal wave in aluminum as a function of laser pulse energy[6]

by vapor of unsteady translational equilibrium and discontinuities in pressure, temperature and density[58]. Beyond the Knutsen-layer is an area of expanding vapor. The incident energy on the vapor leads to a plasma being formed. For high powers, when a critical plasma density is reached, the laser power is absorbed completely by the plasma due to the inverse bremsstrahlung effect and no more energy will reach the materials surface. More vapor is ionized and the plasma expands adiabatic into the direction of the incident laser beam[48]. The stress pulse excited in the ablative regime due to the material vaporization and the heating of the plasma propagates into the material[74].

High energies have not only an influence on the magnitude of waveforms, with scale up to distinct energies linearly but also become more complicated. For higher energies, also the waveform changes with the energy. In Fig. 3.7 the shape of the waveform changes from an impulse to a step. This effect could be explained by shielding effects[38, 48, 27] of a plasma growing with the incident power density.

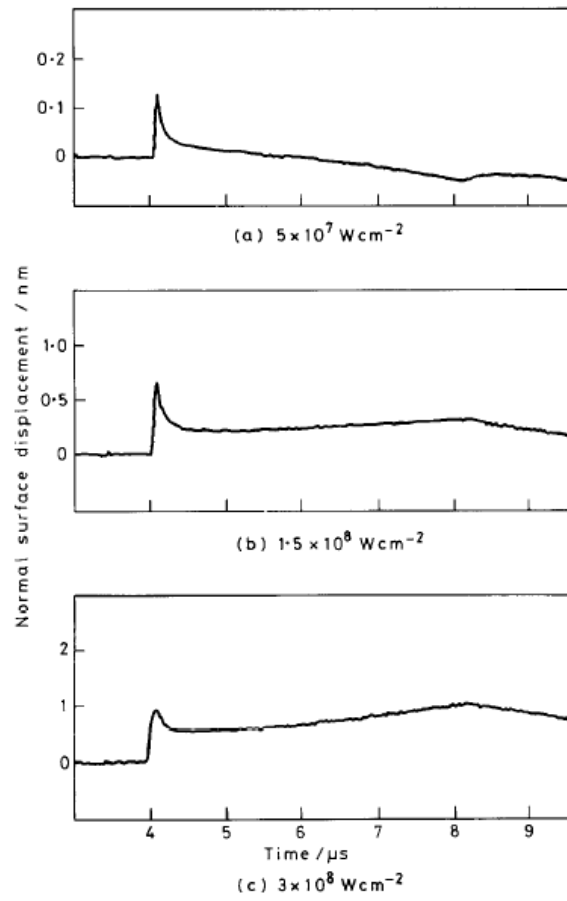


Figure 3.7: Surface wave pulse shape for different excitation energies in the ablative regime[72]

The nonlinear behavior in the nearfield of the ablative source is not only reflected by the nonlinear trend[75, 39] of signal magnitude against laser power, but also in an excitation of higher harmonics, as seen in (Fig. 3.8) where the second harmonic amplitude increases with the laser pulse energy in contrary to the thermoelastic source. A broadened frequency spectrum and the excitation of higher harmonics were also detected by [28] using the ablative laser regime on Silicon single crystals.

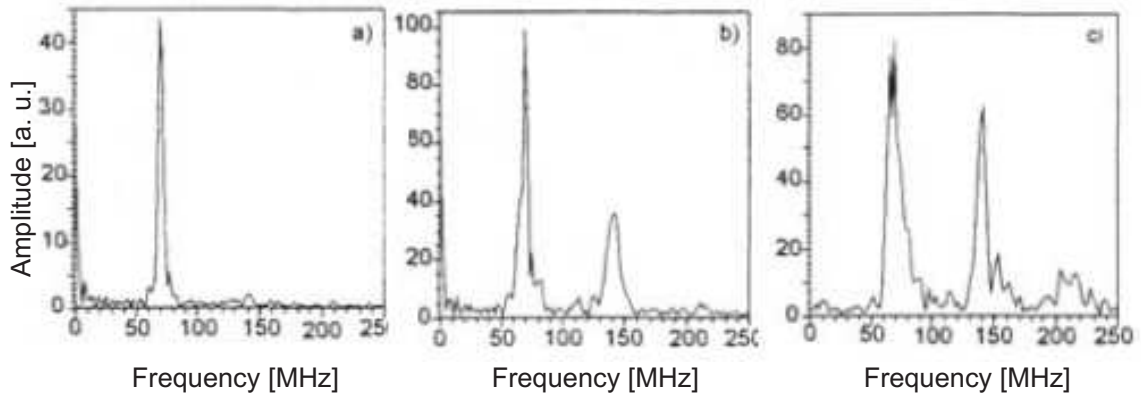


Figure 3.8: Surface wave frequency spectrum for different excitation energies a) 0.5mJ b) 3mJ c) 3.5mJ by narrowband excitation with a pico second laser in the ablative regime[75]

3.2.5 Source Pattern Generation for Narrow Band Signal Excitation

The excitation of a narrow band signal with a laser source, which is in nature broadband is possible by arranging multiple sources in patterns of surface area that is exposed and surface area that is not exposed to the laser illumination. Regular patterns enable narrow band signals, while the shape of the components of the pattern have influence on signal amplitude, directivity, sensitivity[46] and the frequency spectrum.

Different approaches are possible to excite a narrowband wave, using diffraction optics, focusing and diverging lenses and lens arrays and shadow masks.

Multiple Laser Beams [57, 33, 62, 59, 61] The concept of multiple laser beams to excite a harmonic acoustic wave can be used for two different generation methods. An array of laser sources can be used or the beam of a single source can be into several beams. The pattern generation can be due to focusing single beams on the surface[57] or by optical interference[33, 62, 59, 61] of two incident laser beams (Fig 3.9). This technique is flexible according to the desired pattern and has a lot of energetic potential but brings difficulties in the alignment of several laser sources and the interference pattern.

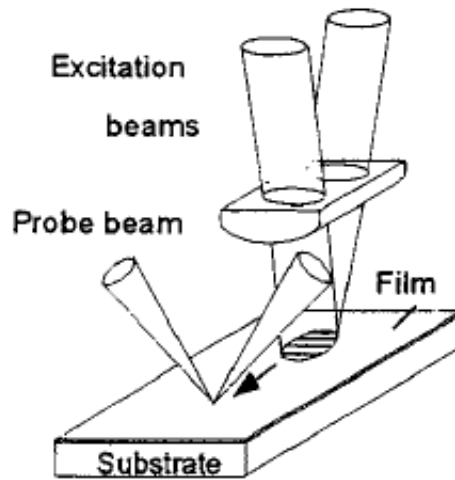


Figure 3.9: Narrowband surface excitation by interference of two incident laser beams[75]

Diffraction Optics [40] The use of diffraction optics like optical gratings and beam splitters (Fig. 4.1) allows an absolute non contact excitation with arrangeable pattern feature sizes and geometries. Transmission gratings have low alignment sensitivity [82]. However the use of systems of focusing and expanding lenses (Fig. 3.10) is necessary to excite a well defined pattern. The pulse energy is limited to the threshold of the diffraction optic and the energy distribution is not uniform over the

pattern[40] and is decreasing strongly with distance from the central feature.

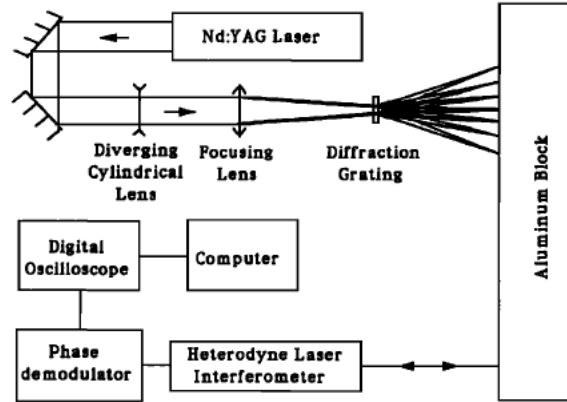


Figure 3.10: Narrowband surface excitation by a diffracted laser beam[40]

Lenticular Array [20, 55] A lenticular array is an array of several focusing lenses (Fig. 3.11) and allows an absolute non-contact excitation method with quasi unlimited use of laser power, the thresholds for focusing optics are much higher for lenses than for gratings. The pattern is inflexible in the amount of features like lines. The line width can be changed by moving the specimen out of the focus of the lenticular array. The signal is very susceptible to misalignment[20].

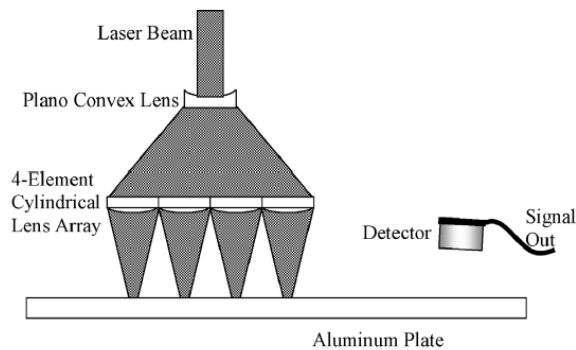


Figure 3.11: Narrowband surface excitation by lenticular array[20]

Shadow Mask [23, 70, 9, 60] The use of a mask to create a source pattern is an approach with an relatively simple set up (Fig. 4.3) and (Fig. 3.12). The alignment is simple and there is almost no limit for the applicable laser pulse energy, as the damage to most materials is very small due to the very short laser pulses. The problematic comes with the fabrication of the masks, as the feature sizes are limited by fabrication process and mask material and the excitable frequency of a narrow-band signal is limited by the manufacturable feature size Eq. 3.18. Furthermore the pattern is not flexible to changes of the pattern. About 50% of the incident energy is lost [20] and the mask has to be attached close to the surface, to avoid diffraction effects[60].

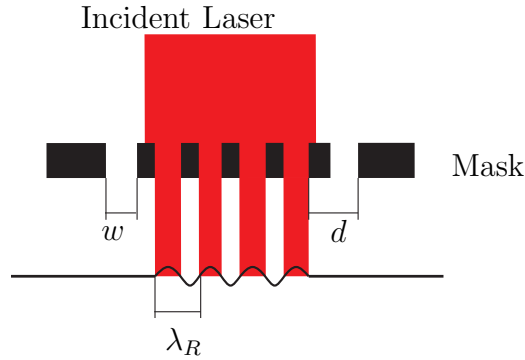


Figure 3.12: Narrowband surface excitation by illumination through a shadow mask[60]

These approaches excite line source patterns on the specimens surface. Against the more simple point source the line source enhances the signal and adds directivity (see Fig. 3.13) to the wave forms [7, 43] and increases the signal to noise ratio[26]. The line focused source also enables the use of higher pulse energies without exciting in the ablative regime [8] as the energy is distributed on a larger surface area. Furthermore [6] reported an increasing wave magnitude of 20% by sharp lateral gradients, such that the excited Rayleigh wave signal is increased by high temporal and

lateral gradients of the thermal source.

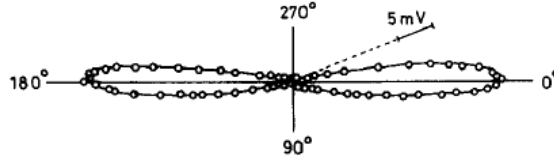


Figure 3.13: Directivity of a laser line source ($4\text{mm} \times 1\text{mm}$) on mild steel[75]

It shall be mentioned that the directivity of the waveform is not the same as the directivity of the energy propagation[55]. Nearfield observations of [26] for thermoelastic sources showed that the line source excites a monopolar Rayleigh wave in the nearfield, while the point source waveform is bipolar. This agrees with the mathematical modulation of the line and point source[4].

A regular line source excites a broadband signal. The narrow band signal is due to several sources that are lined up resulting in a decreasing bandwidth for an increasing number of source elements [23] as seen in Fig. 3.14.

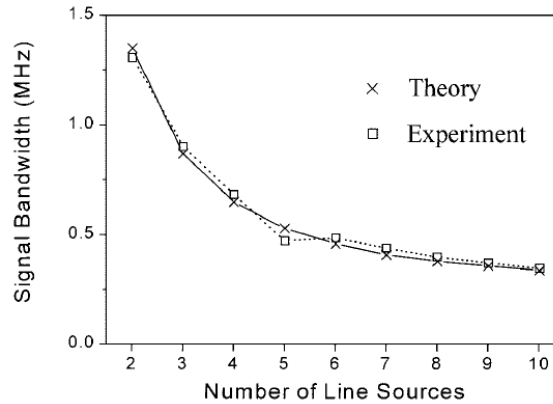


Figure 3.14: Decrement of signal bandwidth with number of line sources[23]

To excite a narrow band signal in the desired frequency, f , the pattern parameters are derived as

$$d = \lambda_R = \frac{2\pi c_R}{\omega} = \frac{c_R}{f} \quad (3.18)$$

with the wavelength of the Rayleigh wave, λ_R , and the Rayleigh wave speed, c_R (Fig. 3.12). These line array parameters essentially control the bandwidth of the signal[20]. For a Gaussian illumination profile of a line source, the source is about 1.65 times larger than the Gaussian radius. Using a diffraction device, the important parameters to illuminate a pattern on a surface is the diffraction angle, θ , and the distance L between the grating and the specimen's surface (Fig. 3.15) . The diffraction angle is determined by

$$\sin \theta_n = \frac{n\nu^r}{p}, n = 0, 1, 2, \dots \quad (3.19)$$

with the slit separation (pitch), p , of the optical grating[35] and the order of the intensity maximum, n . For small angles $\sin \theta_1 \ll 1 \Rightarrow \sin \theta_1 = d/L$ and the distance between specimen and grating is

$$L = d \frac{p}{\nu^r} \quad (3.20)$$

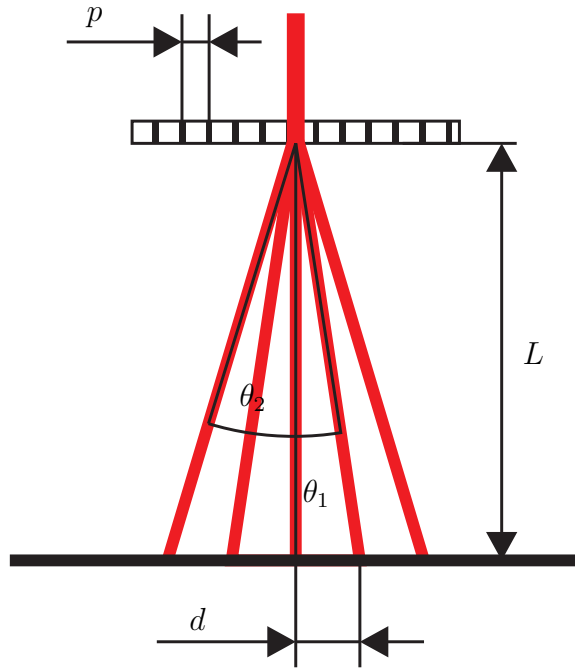


Figure 3.15: Geometric principles of a diffraction grating[23]

3.2.6 Derivation of the Thermoelastic Source

The mathematical modulation of laser generated ultrasound is based on the surface center of expansion theory[73] and is related to a pure mechanical source for the thermoelastic regime. The work of Rose builds the basics for the point source representation in an elastic half space using integral transform techniques[68] and a modulation of a two dimensional line source representation was analyzed by Bernstein and Spicer[13]. A complete model of the laser source valid for near and farfield [54, 79] was made by Spicer[79]. Approaches for a model for a source in the ablative regime were made by [48, 58]. The following derivation of the thermoelastic point and line source is according to Achenbach [4] and is based on the work of the mentioned authors.

For a linearly elastic and isotropic solid, the governing equations for the thermoelastic wave field are given as

$$K\nabla^2 T = \rho c_v \dot{T} + T_0 \beta_c \nabla \cdot \dot{\mathbf{u}} - q \quad (3.21)$$

and

$$\mu \nabla^2 \mathbf{u} + (\lambda + \mu) \nabla (\nabla \cdot \mathbf{u}) = \rho \ddot{\mathbf{u}} \quad (3.22)$$

with the heat conductivity, K , the actual and ambient temperatures, T and T_0 , the mass density, ρ , the displacement vector, $\mathbf{u}(x, t)$, $x = [x_1, x_2, x_3]$, where x_1, x_2 build the surface plane of the half space and x_3 is the positive direction normal into the half space. The thermoelastic coupling constant is $\beta_c = (3\lambda + 2\mu)\alpha$, including the lame constants, λ and μ , and the coefficient of linear thermal expansion, α . The specific heat at constant deformation is c_v and the deposited heat is q . The second term on the right hand side of eq. (3.22) is the heat produced by mechanical deformation and can be neglected for laser generated thermal sources and the equation can be reduced to:

$$\kappa \nabla^2 T - \dot{T} = -\frac{q}{\rho c_v} \quad (3.23)$$

with the thermal diffusivity, $\kappa = K/\rho c_v$. The heat deposition can be expressed as

$$q = E(1 - R)\gamma e^{-\gamma x_3} f(r)g(t) \quad (3.24)$$

with

$$f(r) = \frac{1}{\sqrt{2\pi}} \frac{2}{R_G^2} e^{-2r^2/R_G^2} \quad (3.25)$$

and

$$g(t) = \frac{8t^3}{\nu^4} e^{-2t^2/\nu^2} \quad (3.26)$$

where E is the energy of a laser pulse, R the surface reflectivity and R_G the Gaussian beam radius, ν^t the rise time parameter of the laser pulse and γ the excitation coefficient. r is the coordinate for the Gaussian distribution, represented as a disk where the influence of the laser outside the Gaussian radius is neglected. With the assumption that all energy is absorbed at the surface ($\gamma \rightarrow \infty$) and the limits $\nu^t \rightarrow 0$ and $R_G \rightarrow 0$ the equivalent concentrated point source is

$$q = E(1 - R)\delta(x_3)\frac{\delta(r)}{2\pi r}\delta(t) \quad (3.27)$$

A thermoelastic source in an unbounded medium can be modeled as an equivalent mechanical loading in the form of three mutually orthogonal force dipoles[74]. For the 2-D case and a spatial Gaussian distribution of the laser energy with respect to the x_1 -coordinate(Fig. 3.16), the expression for the deposited heat is

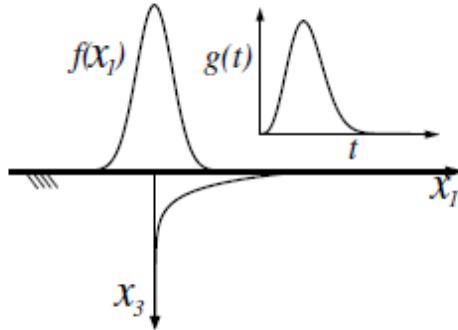


Figure 3.16: Temporal and spatial Gaussian distribution of the laser beam for the 2-D case[8].

$$q = \bar{E}(1 - R)\delta(x_1)\delta(x_3)g(t) \quad (3.28)$$

with the energy in x_2 -direction per unit length. For a infinitesimal element with length l , width δx_2 and depth l_3 :

$$q = \bar{E}(1 - R)\frac{1}{l}\frac{1}{l_3}g(t) \quad (3.29)$$

Using Eq. 3.29 and neglecting the heat conduction, which is according to section (3.2.3) in contrast to Scruby and Drain (1990), reduces Eq. 3.23 to

$$\dot{T} = \frac{\bar{E}}{\rho c_v}(1 - R)\frac{1}{l}\frac{1}{l_3}g(t) \quad (3.30)$$

Representing the temporal distribution by an integration of its harmonic components,

$$g(t) = \int_{-\infty}^{\infty} \hat{g}(\omega)e^{-i\omega t} d\omega \quad (3.31)$$

and the harmonic components of the temperature

$$\delta\hat{T} = \delta T \frac{\hat{g}}{(-i\omega)}e^{-i\omega t} \quad (3.32)$$

with

$$\delta T = \frac{\bar{E}}{\rho c_v}(1 - R)\frac{1}{l}\frac{1}{l_3}. \quad (3.33)$$

δT is the temperature increment leading to thermal expansion of the very thin element with the harmonic components given by Eq. 3.32. In the following the term with the harmonic components of δT which can be derived from Eq. 3.32 will be left out and reintroduced in the end. The element is located on the free surface and maintains plain strain in x_2 . If the element is removed from its surroundings (Fig. 3.17), it will deform freely in the x_1 and x_3 directions and

$$\tau_{11} = \lambda(\epsilon_{11} + \epsilon_{33}) + 2\mu\epsilon_{11} - \beta_c\delta T = 0 \quad (3.34)$$

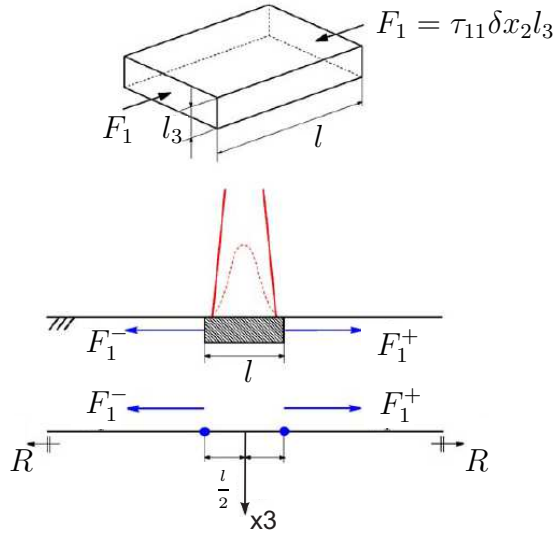


Figure 3.17: Surface element for the derivation of a infinite line source with reaction forces F_1^\pm due to thermal expansion and the excited Rayleigh wave R [4].

$$\tau_{33} = \lambda(\epsilon_{11} + \epsilon_{33}) + 2\mu\epsilon_{33} - \beta_c\delta T = 0 \quad (3.35)$$

yielding to

$$\epsilon_{11} = \epsilon_{33} = \frac{\beta_c\delta T}{2(\lambda + \mu)} = \frac{3\lambda + 2\mu}{2(\lambda + \mu)\alpha\delta T} \quad (3.36)$$

with stress, τ , and strains, ϵ . Putting the element back into the half-space it is compressed in x_1 direction with the amount of the strain, ϵ_{11} . Using this and Eq. 3.35 the strain in x_3 and the stress in x_1 are

$$\epsilon_{33} = \frac{\lambda(3\lambda + 2\mu)}{2(\lambda + \mu)(\lambda + 2\mu)}\alpha\delta T \quad (3.37)$$

and

$$\tau_{11} = -\frac{2\mu}{\lambda + 2\mu}(3\lambda + 2\mu)\alpha\delta T \quad (3.38)$$

The forces that are produced due to this stress that generate the ultrasonic wave in the half-space in $\pm x_2$ direction (Fig. 3.17) results in

$$F_1^\pm = \pm \tau_{11} l_3 = \pm \frac{\bar{D}}{l} \quad (3.39)$$

These forces work at $\pm l_2/2$ with the dipole per unit length, \bar{D} , defined by the double force:

$$\bar{D} = \frac{2\mu}{\lambda + 2\mu} (3\lambda + 2\mu) \alpha \frac{\bar{E}}{\rho c_v} (1 - R). \quad (3.40)$$

In the axial symmetric case for a finite point source of radius r_0 the volume element has the shape of a thin disk (Fig. 3.18) and Eq. 3.33 is rewritten as

$$\delta T = \frac{E}{\rho c_v} (1 - R) \frac{1}{\pi r_0^2} \frac{1}{l_3} \quad (3.41)$$

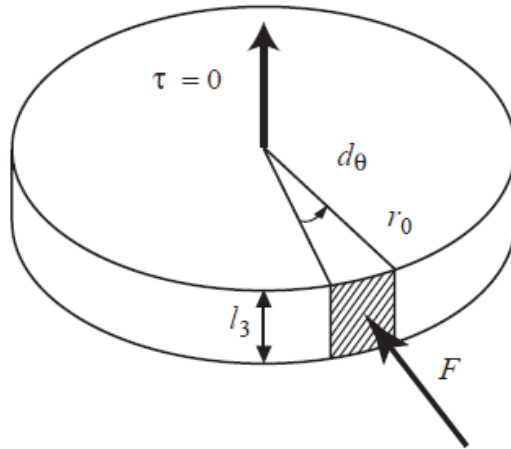


Figure 3.18: Surface element for finite point source[4].

and for the radial strain of the free element

$$\epsilon_r = \epsilon_{33} = \epsilon_\theta = \alpha \delta T. \quad (3.42)$$

Placing the disc back in the half-space and the application of the boundary conditions yield to

$$\epsilon_{33} = \frac{2\lambda\alpha\delta T}{\lambda + 2\mu} \quad (3.43)$$

and

$$\tau_{rr} = -\frac{2\mu}{\lambda + 2\mu}(3\lambda + 2\mu)\alpha\delta T \quad (3.44)$$

and the radial Force

$$F_r = \frac{D}{\pi r_0^2} \quad (3.45)$$

where $D = \bar{D}$. Arias and Achenbach (2003) showed that for a set of point sources ($r_0 \rightarrow 0$) the surface tractions are equivalent to a set of orthogonal dipoles of magnitude D on the surface of the half-space (Fig. 3.19).

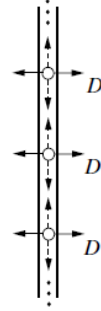


Figure 3.19: Schematic superposition of force dipoles for a line source[8].

A more general derivation for transversely isotropic materials was made by Achenbach (2005)[5].

From above we know that the radiated surface has an equivalent mechanical loading of forces due to orthogonal dipoles and a set of body and surface waves are excited. In sufficient distance only the surface disturbances are of any interest due to the faster decay of the body waves[4]. The time harmonic forces Eq. 3.39 and Eq. 3.45 and taking the displacements also with the time harmonic factor $[\hat{g}(\omega)/(-i\omega)]exp(-i\omega t)$ the boundary conditions at the surface $x_3 = 0$ are

$$\tau_{31} = -F_1^+ \delta(x_1 - \frac{l}{2}) + F_1^- \delta(x_1 + \frac{l}{2}), \quad (3.46)$$

$$\tau_{33} = 0, \quad (3.47)$$

and no heat transport across the boundary

$$\frac{\partial T}{\partial x_3} = 0 \quad (3.48)$$

The displacement and stress components depend only on x_1 and x_3 with a still omitted time-factor. For the solution the technique of reciprocity theorem for elastodynamics [3] connected with the virtual wave[1], where a surface wave propagating on a free surface is represented by a carrier wave of motions of exponentially decay for increasing x_3 . The displacements in terms of the carrier wave $\phi(x_1, x_2)$ where $\phi = \exp(-ik_R x_1)$ for $x_1 > 0$ and $\phi = \exp(ik_R x_1)$ for $x_1 < 0$

$$u_1 = A \frac{1}{k_R} V^R(x_3) \frac{\partial \phi}{\partial x_1}(x_1, x_2), \quad (3.49)$$

$$u_2 = A \frac{1}{k_R} V^R(x_3) \frac{\partial \phi}{\partial x_2}(x_1, x_2) \quad (3.50)$$

and

$$u_{x_3} = A W^R(x_3) \phi(x_1, x_2) \quad (3.51)$$

with the wave number, $k_R = \omega/c_R$, and the Rayleigh velocity, c_R . The condition for the carrier wave is:

$$\frac{\partial^2 \phi}{\partial x_1^2} + \frac{\partial^2 \phi}{\partial x_2^2} + k_R \phi = 0 \quad (3.52)$$

where V^R and W^R are determined by Eq. A.3 and Eq. A.4.

The elastodynamic reciprocity theorem for the half-plane, V , with $x_3 \geq 0$ with a

boundary, S , which is defined by $x_3 = 0$, and the lines $x_1 = a$ $x_1 = b$ and $x_3 \rightarrow \infty$ (with no contribution) and two time-harmonic states, A and B , is

$$\int_V (f_j^A u_j^B - f_j^B u_j^A) dV = \int_S (\tau_{ij}^B u_j^A - \tau_{ij}^A u_j^B) n_i dS \quad (3.53)$$

with the outward normal donated by \mathbf{n} . For the state A , surface waves are selected such that propagate from the source into the positive and negative x_1 direction

$$u_1^A(x_1, x_2) = \pm i A V^R(x_3) e^{\pm i k_R x_1}, \quad (3.54)$$

$$u_3^A(x_1, x_2) = A W^R(x_3) e^{\pm i k_R x_1} \quad (3.55)$$

with amplitude A of the surface wave and the relevant related stresses

$$\tau_{11}^A(x_1, x_3) = A T_{11}^R(z) e^{\pm i k_R x_1}, \quad (3.56)$$

$$\tau_{13}^A(x_1, x_3) = \pm i A T_{13}^R(z) e^{\pm i k_R x_1}, \quad (3.57)$$

with T_{11}^R and T_{13}^R defined by Eq. A.10 and Eq. A.11. For state B , the virtual wave propagating in the positive x_1 -direction and amplitude B is described by:

$$u_1^B(x_1, x_2) = i B V^R(x_3) e^{i k_R x_1}, \quad (3.58)$$

$$u_3^B(x_1, x_2) = B W^R(x_3) e^{i k_R x_1}, \quad (3.59)$$

$$\tau_{11}^B(x_1, x_3) = B T_{11}^R(z) e^{i k_R x_1}, \quad (3.60)$$

$$\tau_{13}^B(x_1, x_3) = i B T_{13}^R(z) e^{i k_R x_1} \quad (3.61)$$

For this problem the reciprocity relation from Eq. 3.53 becomes

$$iB\bar{D} \left[\frac{1}{l} e^{ik_R l/2} - \frac{1}{l} e^{-ik_R l/2} \right] = \underbrace{\int_{\infty}^0 F_{AB}|_{x_1=b} dx_3}_{=0} - \underbrace{\int_0^{\infty} F_{AB}|_{x_1=a} dx_3}_{=2iABI} \quad (3.62)$$

with

$$F_{AB} = u_1^A \tau_{11}^B + u_3^A \tau_{13}^B + u_1^B \tau_{11}^A + u_1^B \tau_{11}^A \quad (3.63)$$

and I from Eq. A.15. The integrations along $x_1 = a, 0 \leq x_3 \leq \infty$ and $x_1 = b, 0 \leq x_3 \leq \infty$ yield only contributions from counter propagating waves which is at the present choice for $x_1 = a, 0 \leq x_3 \leq \infty$ and for the limit of $l \rightarrow 0$ Eq. 41 turns into

$$k_R B \bar{D} V^R(0) = 2iABI \quad (3.64)$$

and the amplitude of the dipole force generated surface wave is

$$A(\omega) = \frac{k_R \bar{D} V^R(0)}{2iI} = -\frac{i\omega}{c_R} \frac{V^R(0)}{I} \frac{\bar{D}}{2}. \quad (3.65)$$

Eq. 3.65 into Eq. 3.55 and reintroduction of the time factor gives

$$\hat{u}_3(x_1, \omega) = -\frac{1}{c_R} \frac{V^R(0) W^R(0)}{I} \frac{\bar{D}}{2} \hat{g}(\omega) e^{\pm ik_R x_1 - i\omega t} \quad (3.66)$$

and by using Eq. 3.31 and assuming that the Rayleigh pulse has the same temporal dependency like the laser pulse, the normal displacement at the surface results in:

$$u_3(0, t) = -\frac{1}{c_R} \frac{V^R(0) W^R(0)}{I} \frac{\bar{D}}{2} g(t \mp x_1/c_R) \quad (3.67)$$

For an array of lines it is assumed, it is assumed that the generated wave $h(t)$ of a single line source travelling in positive x_2 direction scales in the farfield like

$$h(t) \propto (x - c_R t) e^{-4(x-ct)^2/d} \quad (3.68)$$

with a frequency representation

$$H(f) \propto f e^{\pi^2 f^2 d^2 / 4c_R^2} \quad (3.69)$$

where d is the characteristic width of the Gaussian distribution (intensity drops to $1/e$ of the maximum value). For an array of N lines with Gaussian distribution the wave can be described in time domain as

$$g(t) = \sum_{n=1}^N h(t - n\delta t) \quad (3.70)$$

and respectively the frequency spectrum

$$G(f) = NH(f)S(f), \quad (3.71)$$

with the propagation time between two successive line sources and

$$S(f) = \frac{\sin(\pi N f \delta t)}{N \sin(\pi f \delta t)}. \quad (3.72)$$

The fundamental frequency of the excited signal is $f_0 = 1/\delta t$ with a signal bandwidth of $2f_0/N$ and for the array function (Eq. 3.72) principle peaks of narrowband character at $f_n = (n + 1)f_0$ [40].

3.2.7 Derivation of the Ablative Source

The most difficulties of the derivation of a mathematical model of the ablative source are due to the effects during the interaction of plasma and laser beam[27] and the fact that the thermal constants vary for high temperatures as well as for the liquid and gaseous phase[10].

As mentioned above the ablative source can be equivalent modeled as a force acting normal on the surface into the material, mainly excited by the removed material. The effects of thermoelastic strains can be neglected, when the absorbed power density I' is above the critical power density

$$I_c \geq 2Q\rho\sqrt{\kappa/\tau} \quad (3.73)$$

with the latent heat, Q , required to vaporize the solid and the stress resulting from the repelled material can be calculated by Newton's second law of motion as the rate of the change of the momentum[74]:

$$\sigma = \frac{I\zeta}{Q + C(T_v - T_0)} \quad (3.74)$$

with the vaporization and initial temperatures T_v and T_0 , and the rate of removed material ζ . The determination of ζ depends mainly on the incident power and pulse length τ [74]. For not Q-switched lasers with relatively long laser pulses ($\tau \sim 10^{-3}s$, ζ is

$$\zeta = \frac{I'}{\rho[L + C(T_v - T_0)]} \quad (3.75)$$

and Eq. 3.74 results in

$$\sigma = \frac{I^2}{\rho[Q + C(T_v - T_0)]^2}. \quad (3.76)$$

Eq. 3.76 takes only the influence of the free repelled material into account. However for short laser pulses, due to the probability of material getting ejected in the liquid phase and influences of the plasma the derivation of the ablative source becomes complicated. The plasma puts pressure on the molten and vaporized phase and prevents ejection but keeps inducing heat into the surface. Therefore material is vaporized even after the end of the laser pulse[10] for a long time. The variation

of the resulting stresses is between two limiting cases: The resulting stress has the temporal form of the laser pulse (see Eq. 3.26) and a heavy-side unit-step function $H(t)$. [10] therefore describes the boundary conditions for a ablative source on the surface at $x_3 = 0$ for a point source as

$$\sigma_{33} = f_a \frac{\delta(r)}{2\pi r} \begin{cases} \delta(t) \\ H(t) \end{cases} \quad (3.77)$$

due to a force with amplitude f_a varying in temporal form between pulse and step shape.

Such the characteristics of the ablative source depend on laser intensity and pulse width, the wavelength of the laser light and the plasma parameters, which essentially determine the energy transport and the momentum on the surface[48]. [44] developed a simulation model for the ablative regime.

CHAPTER IV

EXPERIMENTAL SETUP

In section 3.2.5 four different techniques to generate a narrow band ultrasonic signal were presented. The diffraction optics and shadow mask techniques were the most promising methods to excite the desired signal for harmonic generation and investigation of the non-linear ultrasonic behavior of materials based on the available equipment. The technique should be able to excite wave signals of a frequency above 1 MHz . According to Eq. 3.18 the distance between two excitation lines of a Rayleigh wave ($f > 1 MHz$) on common metals is smaller than three mm and decreases with increasing frequency. Two different set ups had to be developed to address different problems.

4.1 Laser

The used emission source is the Surlite I-10 from Continuum. An introduction to laser principles was given in section 3.2. The Surelite I-10 is a Q-switched Nd:YAG (neodymium-doped yttrium aluminum garnet; $Nd : Y_3Al_5O_{12}$) laser and is used to emit radiation of 1064 nm wavelength. The pulse width is 5 ns – 7 ns and the Rod diameter of the Gaussian shaped beam is 6 mm with a divergence of 0.6 $mrad$ s. The energy of the emitted laser pulse is 460 μJ . The frequency for the flash lamp discharge was 5 Hz with a discharge voltage of 1.24 kV per discharge and the Q-switch delay was 188 μs for maximum energy output. The Surelite I-10 has a flash lamp discharge divider, which allows the user to change the emission frequency of the laser without changing the discharge frequency of the flash lamp as well as enables single shots.

4.2 Diffraction Grating Set Up

The use of pattern generation by diffraction optics is based on the physical principles of the diffraction of electromagnetic radiation (Section 3.2.5). There the incident laser beam is diffracted and a theoretical endless pattern of the same spatial shape as the incident beam is generated. This technique uses diffraction devices such as diffraction gratings, beam splitters and diffusers. The naming of this kind of optics does not seem to be constant but depends on the manufacturer. To enhance the quality of the generation and enable higher first harmonic frequencies, the laser beam has to be manipulated in shape and intensity by the use of convex and concave, cylindrical and spherical lenses (Fig. 4.1).

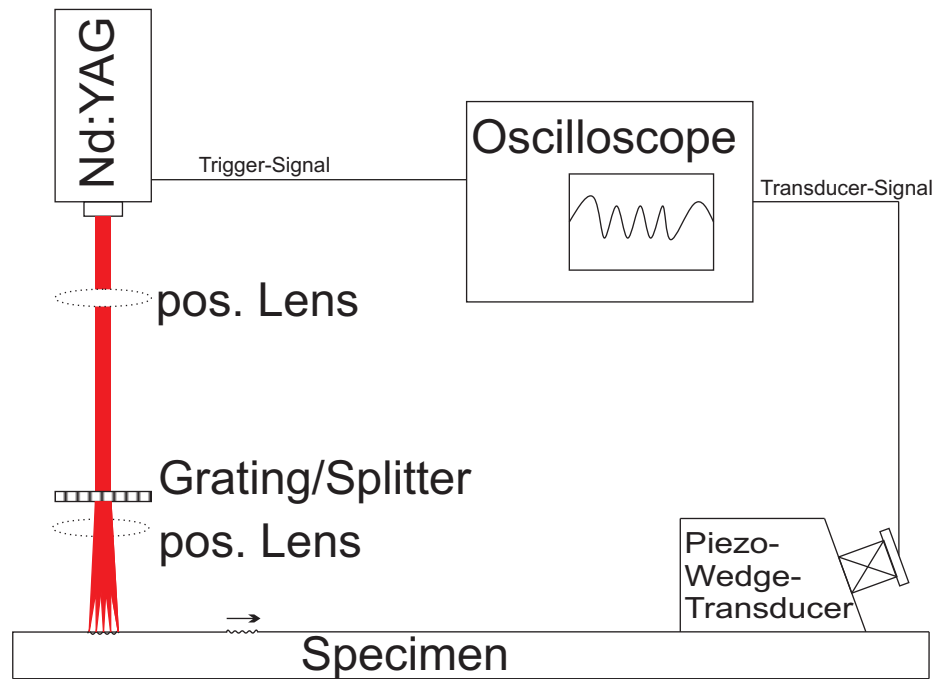


Figure 4.1: Illumination pattern for narrowband signal excitation by diffraction optics and different sets of focusing lenses. The signal is detected by a conventional wedge-transducer

In Fig. 4.1 two different positions for additional optics are marked. Therefore it

is possible to create spatial separated point and line sources with a sharp focus. The additional optics are necessary to reduce the spot size of the emitted laser from $6mm$ to a usable size, since the width of the illuminated feature on the surface should be approximately half the desired wavelength λ_R .

In contrast to the set up of Huang et al. (1992) (Fig. 3.10), the manipulation of beam diameter and shape was made after the beam got diffracted. This optical set up design was necessary because of the experiments high energy pulse and the risk associated with focusing, namely damaging the diffraction device by increasing the power density of the laser pulse.

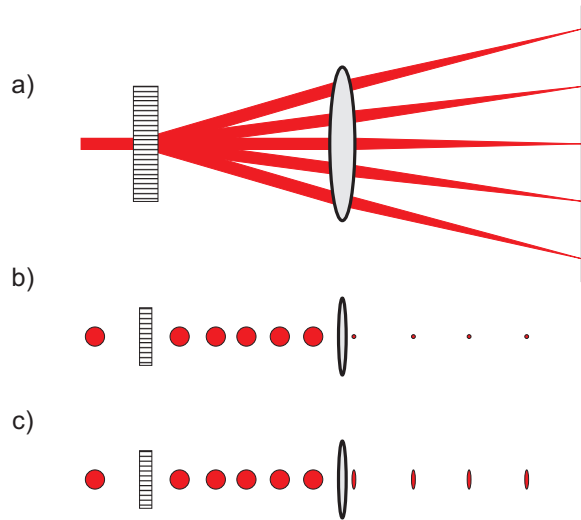


Figure 4.2: a) Diffraction and focusing of laser beam for b) pattern of point sources by a spherical lens and c) pattern of line sources by a cylindrical lens

Optics For the optical bench like in Fig. 4.2 the following optics were available (Tab. 4.1). The distances between the diffraction optic and the specimen can be calculated by Eq. 3.19 and Eq. 3.20. The distance between lens and specimen is empirically optimized, as slightly out of focus alignment can increase the amplitude[30] and is more gentle to the specimens surface, due to lower peak power densities.

Table 4.1: Optics for diffraction and beam manipulation

Diffraction Optics	Beamsplitter I	Pattern of 15 lined up dots. Full angular divergence is 2.7° . Made of SiO_2 for a higher damage threshold. Efficiency of 72%. (MEMS Optical, Inc., Product number: 1017)
	Beamsplitter II	Pattern of 10 lined up dots. Full angular divergence is calculated to $\sim 5.7^\circ$. Made of SiO_2 for a higher damage threshold. Efficiency is unknown. (MEMS Optical, Inc., Product number: <i>unknown</i>)
	Diffuser	Pattern of 25 lines. The diffuser is made of SiO_2 for a higher damage threshold. Full angular divergence in horizontal and vertical is 10.7° and the divergence of the lines is 0.2° . (MEMS Optical, Inc., Product number: <i>D056</i>)
	Transmission Grating	Near IR Transmission Grating. 300 grooves (lines/mm). Size $50 \times 50mm$ (Thorlabs, Product number <i>GTI50 - 03</i>)
Lenses	Spherical lens	Focal length of $\sim 12cm$ (unknown origin)
	Cylindrical lens	Focal length of $10mm$ (Edmund Optics Inc., Product number: <i>NT48 - 360</i>)

4.3 Shadow Mask Set Up

The shadow mask creates a direct pattern on the specimen's surface. The mask parameters are determined in Eq. 3.18 and by the assumption, that the slit width of the mask should be about half the wavelength λ_R . According to [23] the optimal slit width w of a shadow mask for laser ultrasonics for narrowband excitation in the thermoelastic regime is

$$w = \frac{\sqrt{2}\lambda_R}{\pi} \approx 0.45\lambda_R \quad (4.1)$$

with the desired acoustic wavelength λ . According to the different excitation processes masks with different slit widths in the range of approximately $\frac{\lambda}{2} \pm 30\%$ were manufactured. The fabrication accuracy depends on mask material and feature size. Different materials were tested in terms of permeability to the emitted radiation from the laser ($\nu^r = 1064 \text{ nm}$) and manufacturability for the small feature sizes. Among others polyethylene, plastic, colored acrylic plates, and cardboard were under examination. For fabrication of the small slit pattern the IR-laser cutter from the Georgia Tech Invention Studio was used. While the acrylic plate had the best cutting performance it is opaque to the laser-light. Some plastics proved not to be ideal since they were destroyed and melted after multiple laser pulses. The cardboard had good laser absorbing properties without damaging itself too much. Furthermore the Invention Studio had a lot of experience in cutting cardboard and the fabrication of masks with a slit width of beyond $150 \mu\text{m}$, which corresponds to an excited acoustic frequency of $\approx 10 \text{ MHz}$ in steel and aluminum, was possible. The quality check was made by a metric measurement scale included in a magnification glass. Therefore it was possible to examine the slit separation d but it was not possible to determine the exact slit width w on this method. The calculated values for the two specimen materials are $d = 0.58 \text{ mm}$ for aluminum and $d = 0.6 \text{ mm}$ for steel. The thickness of the cardboard was about 0.8 mm . For a narrow band signal it is important to maximize the number of lines in the illuminated pattern. This is made possible by using higher frequencies and by expanding the laser beam (Fig. 4.3). For this purpose a beam expander (Edmund Optics Inc., Part-#*NT48-360*) was used. The expander is variable and expands incident laser beams in the range of $\times 1$ to $\times 3$ and can also be used as a focusing or diverging lens through special adjustments.

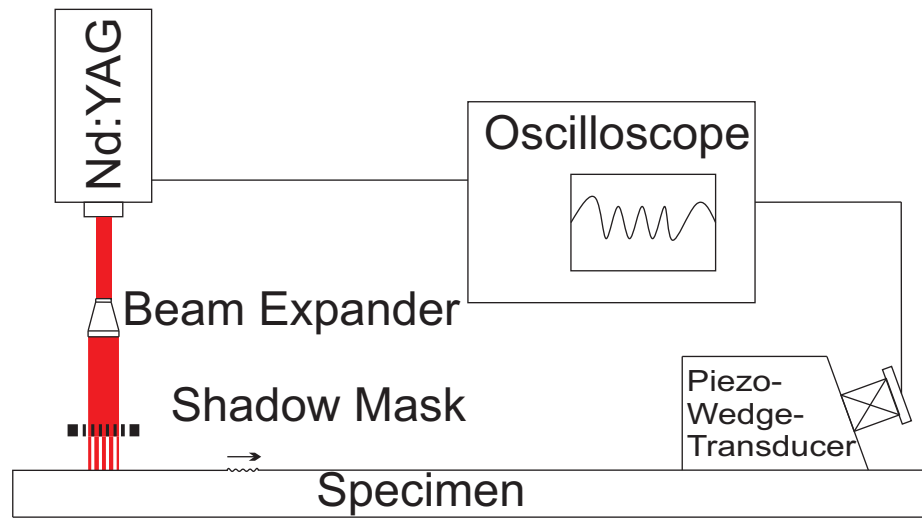


Figure 4.3: Illumination pattern for narrowband signal excitation by a shadow mask. The signal is detected by a conventional wedge-transducer

4.4 *Specimen*

The specimens used for the experiments were dog boned shaped steel specimens (A36) and an Aluminum (Al 6061) plate. The A36 steel specimen and the aluminum plate were used for basic investigations of the characteristics of the excited signal in thermoelastic and ablative regime. Walker et al. (2011) used in previous experiments the A36 specimens to detect fatigue damage in steel by the use of non-linear Rayleigh surface waves. An increasing non-linearity with number of fatigue cycles was shown [78]. These specimens were used to compare the results of the non-linearity measurement by contact excitation with those by the new non-contact laser generation method.

In the experiments the specimens were clamped to a linear actuator with their surface perpendicular to the incident laser beam. While the incident angle of the laser beam has no influence on the energy absorption[64] misalignment can lead to uneven illumination for diffraction techniques and reduction of linewidth due to the thickness of the mask material in the mask technique. The measurements for the signal behavior against the distance were performed by moving the specimen by the actuator. For

repeated measurements on the steel specimen a surface treatment and polishing is necessary between every set of measurements. The aluminum plate was large enough to perform several measurements.

4.5 *Signal Detection*

While for a complete non-contact method the detection can be realized by the use of optical detection methods, EMAT transducers or air coupled transducers (Section 3.1) the focus of this work was on the non-contact excitation. Therefore the ultrasonic signal was detected by an piezoelectric wedge transducer (Tab. 4.2) . A piezoelectric transducer (Tab. 4.2) was attached to a Plexiglas wedge with angle $\theta = 70^\circ \pm 1^\circ$, which depends on the linear characteristics of the material and can be derived by Snell's-law in the form

$$\frac{\sin \theta_1}{\sin \theta_2} = \frac{c_1}{c_2} \quad (4.2)$$

and results in $\theta_{Aluminum} \approx 68^\circ$ and $\theta_{Steel} \approx 65^\circ$ for a longitudinal wave speed in Plexiglas, $c_L^{Plexiglas} = 2720 \text{ m/s}$. The center frequency of the receiving transducer twice the excitation frequency is necessary to sense the second harmonic component. The detected signal was stored by an oscilloscope (Tektronix TDS 420) with a sample rate of $100MS/s$. For some of the measurements an additional high pass filter was used. The oscilloscope was externally triggered by the laser control unit and the signal's output is in Volts.

Table 4.2: Piezoelectric Transducers

Transducer	Characteristics
Panametrics A109S (# 527408)	Narrowband transducer (5 MHz center freq.) 0.5" in diameter
Panametrics V112 (# 823918)	Broadband transducer (10MHz center freq.) 0.25" in diameter

4.6 Signal Processing

Fig. 4.4 shows the time domain signal of the excited 5MHz tone-burst. Due to the small number of cycles and the Gaussian shape of the burst signal, no further windowing techniques are applied and a fast Fourier transform is performed on the signal. In the resulting frequency spectrum the first harmonic and second harmonic components (A_1 and A_2) are determined. In terms of non-linear wave propagation the non-linearity parameter β is determined and plotted against the propagation distance.

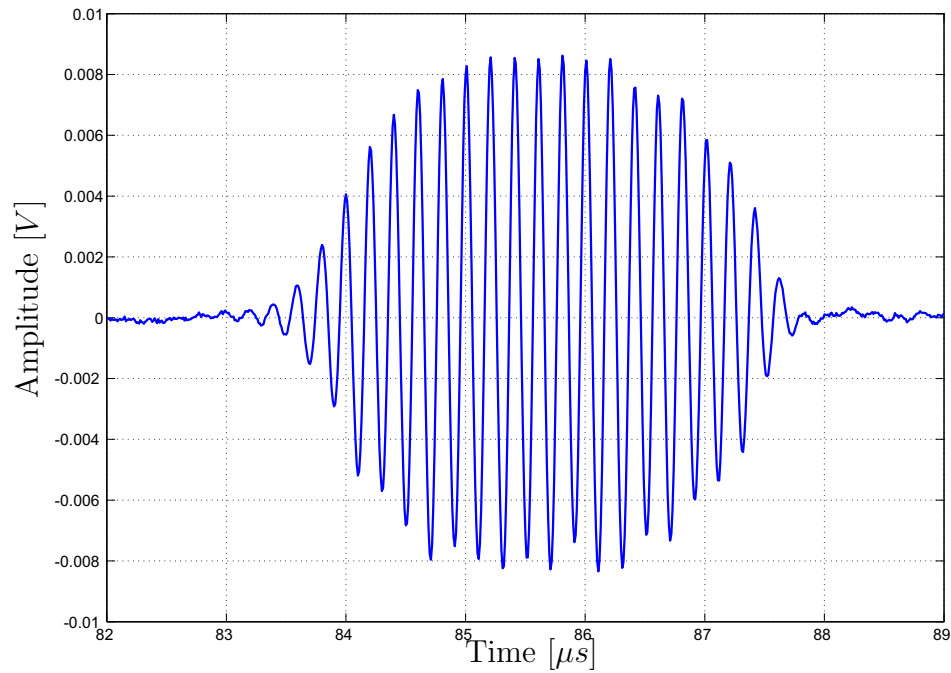


Figure 4.4: 5MHz Narrowband tone-burst signal by mask illumination

CHAPTER V

EXPERIMENTAL RESULTS

The goal of the research is to develop and characterize a noncontact harmonic excitation method for Rayleigh surface waves using the laser described in section 4.1. Two possible approaches are introduced in sections 4.2 and 4.3. In the experiments it is first determined, which technique is capable to generate a harmonic narrowband surface wave signal, that is sufficiently strong to observe material nonlinearities. Then the more suitable shadow mask technique is used to excite harmonic signals to measure the expected increasing nonlinearity parameter for increasing propagation distance (Section 2.3).

5.1 Harmonic Signal Generation

For the determination of the necessary pattern parameter for both specimen materials (Section 4.4) and as verification that the measured signal is the Rayleigh wave, the speed of the generated wave is measured. For this purpose a pulse train of signals is generated by focusing the beam on the specimens surface using a cylindrical lens. Averaging from seven measurements and $c = \Delta s / \Delta t$ results in $c_R^{Alu} = 2940 \text{ m/s}$. This is in good agreement with the literature value for aluminum, $c_R^{Alu} = 2930 \text{ m/s}$. Similarly for steel: $c_R^{Steel} = 3003 \text{ m/s}$ (Lit.: $c_R^{Steel} = 3000 \text{ m/s}$).

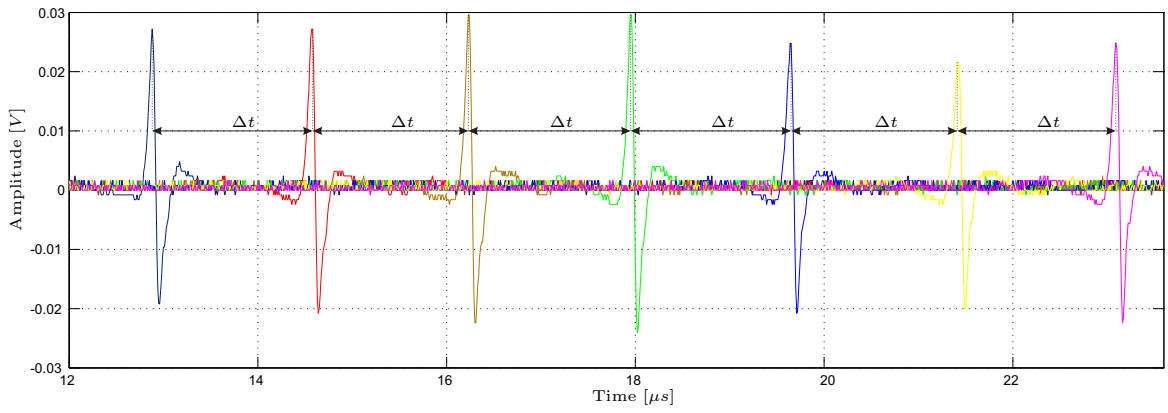


Figure 5.1: Measurement of Rayleigh wave speed on aluminum. Seven measurements with distance $\Delta s = 5 \text{ mm}$

5.1.1 Signals Generated by Diffraction Optics

For Beamsplitter I (Tab. 4.1) the calculated distance (comparable to Fig. 3.15) is $L = 17.8 \text{ cm}$. In Fig. 5.2 the diffracted beam is focused with the spherical lens (focal length $\approx 12 \text{ cm}$) on the surface of the specimen. The signal has a length of fifteen cycles as expected. Slight out of focus alignment can increase the magnitude of pulse signals[30]. In Fig. 5.2 b) the lens is moved that the specimen is out of focus for $\sim 1.5 \text{ mm}$. As a result the signal pattern seems to be more uniform besides the maximum caused by the center point of the excitation pattern then the in focus signal. Further out of focus alignment increases the amplitude but distorts the signal's shape(Fig. 5.2).

It is not possible with the described set up to excite a signal without the strong pulse in the signal's center. The reason is the energy distribution during the diffraction process. Unfortunately MEMS Optics is not able to provide any product information about the energy distribution of the beam splitters. According to [24] the energy distribution of beam splitters is $\approx 25\%$ to the diffraction maximum of 0-th order and $\approx 25\%$ on the maxima of first order. The use of Beamsplitter II (Tab. 4.1) with an even number of spots showed a strong anti harmonic behavior in the signal's center. The reason therefore could be that the grating diffracts only part of the incident

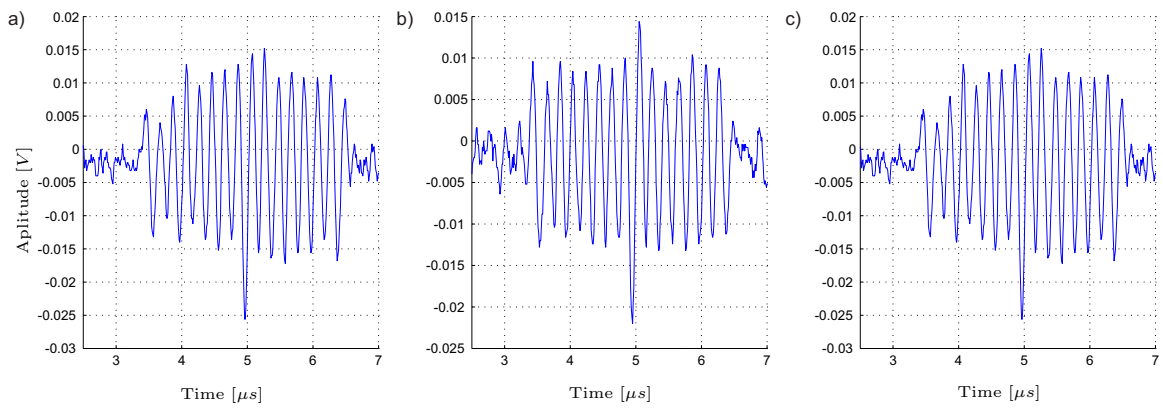


Figure 5.2: 5 MHz Narrow band signal excitation by Beamsplitter on steel a) in focus, b) 1.5 mm out of focus, c) 5 mm out of focus.

beam and transmits the other part undiffracted. For an odd number of maxima spots produced by the diffraction device, the center spot coincides with the 0th-order maximum, while for an even number of spots the undiffracted beam is between the two maxima of first order. Using a cylindrical lens (Fig. 5.3) enhances the ratio between the center maximum and the rest of the cycles. Furthermore the excited signal looks more like a chain of mono-polar pulses, as compared to the signals in Fig. 5.2.

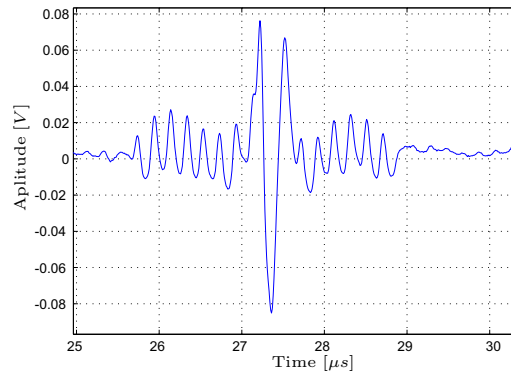


Figure 5.3: 5 MHz Narrow band signal excitation by Beamsplitter line focused on steel with a cylindrical lens.

The use of the Diffuser (Tab. 4.1) did not improve the signal at all. The illuminated line pattern behaves as a source that is assumed to be thermoelastic and excites a signal on top of a strong pulse (Fig. 5.4)

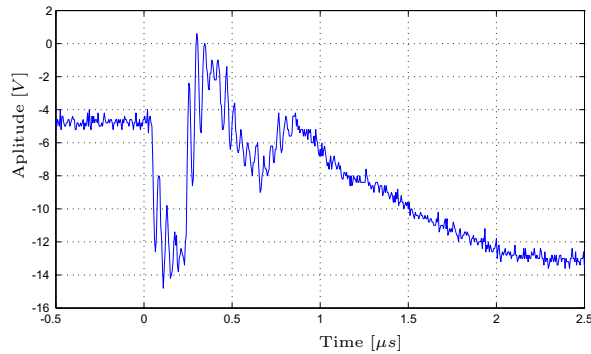


Figure 5.4: 5 MHz Signal excitation by Diffuser (no additional focusing optics).

The use of the Transmission Grating (Tab. 4.1) did not result in any harmonic excitation. Due to the fine pitch ($\sim 3.3 \text{ mm}$) the diffraction angle was very large and the linearization for Eq. 3.20 is not valid any more. Furthermore the threshold of the grating was too low for the power density of the laser pulse and a damage was visible on the gratings surface.

5.1.2 Signals Generated by Shadow Mask

For the diffraction technique, the wavelength of the excited signal determined by the distance between grating and specimen, while the amount of line and point sources depends on the diffraction device itself. For shadow masks, the amount of line sources depends on the amount of slits that are illuminated by the laser while the excited wavelength is unique for every mask. One way to increase the illuminated number of slits is to expand the spatial profile of the laser beam. Another way is to use smaller mask feature sizes d and w (Fig. 3.12) that will excite a higher frequency. In Fig. 5.5 the mask parameters are $d = 1.5 \text{ mm}$ and $w = 0.75 \text{ mm}$. The laser beam is unexpanded. The excitation source has a spatial spread of 4–5 wavelengths.

The propagation distance was very short ($2 - 3 \text{ cm}$). The signal was detected by a narrowband transducer with center frequency at 5 MHz (Tab. 4.2) and the high excitation of the second harmonic with a ratio of $\frac{A_1}{A_2} = 7.8$ in the nearfield for an ablative source coincide with observations of [75].

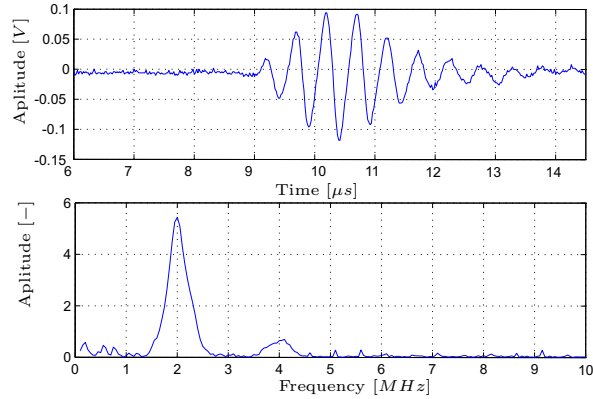


Figure 5.5: 2 MHz signal excitation by shadow mask and a beam diameter of 6 mm .

To increase the number of cycles, the parameters of the masks are changed to $d = 0.6 \text{ mm}$ and $w \approx 0.3 \text{ mm}$ corresponding to a excited frequency of $\sim 5 \text{ MHz}$. Furthermore, the laser beam is expanded by a beam expander (Tab. 4.1) to double the spatial diameter. In Fig. 5.6 the signal is detected in the nearfield with a 10 MHz broadband transducer (Tab. 4.2).

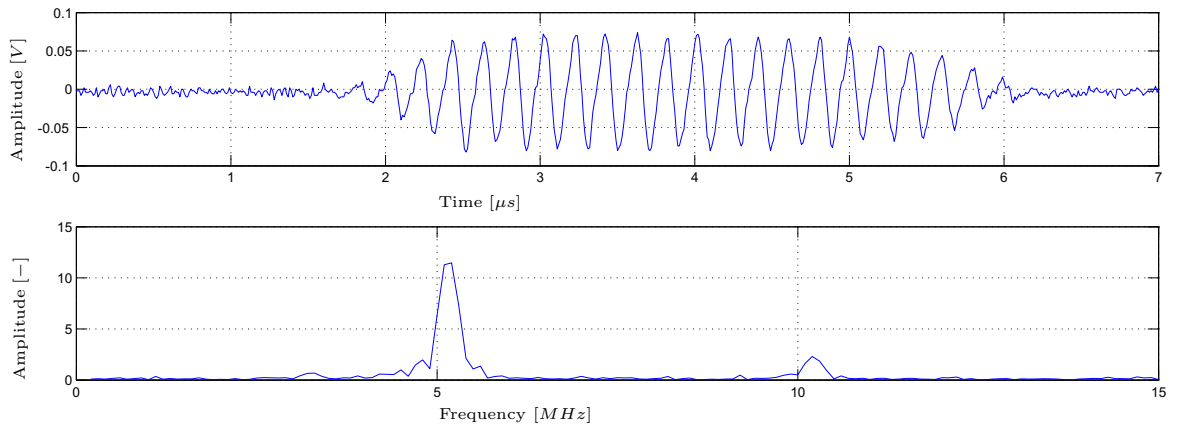


Figure 5.6: 5 MHz signal excitation by shadow mask and $\times 2$ expanded laser beam.

Figures 5.5 and 5.6 show recordings of single shot measurements. Since the small signal amplitudes in laser ultrasonics the signal for nonlinearity measurements is averaged. Fig. 5.7 shows a typical signal used for the detection of the second harmonic. The signal was recorded with a 10 MHz broadband transducer and averaged for 32 separate laser shots. The signal-to-noise ratio is $SNR \approx 9.6$

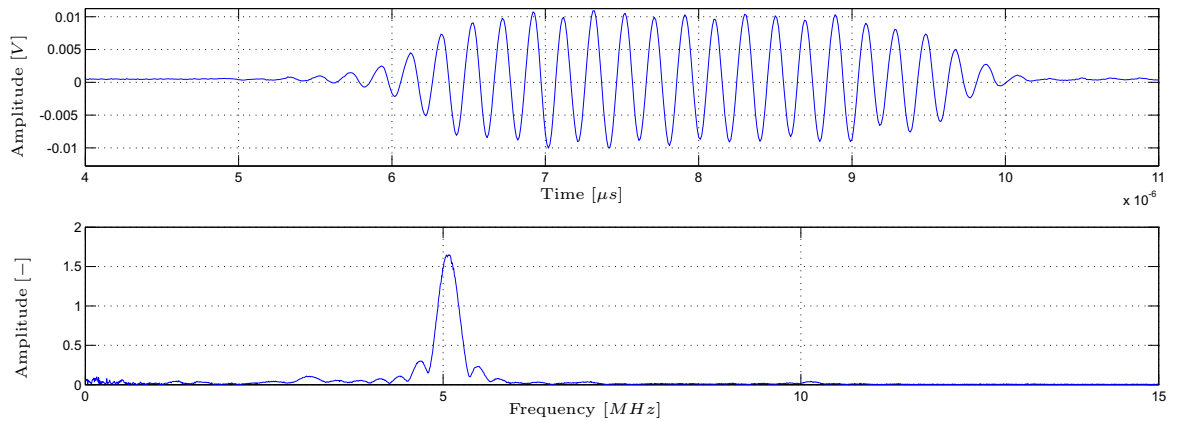


Figure 5.7: Averaged signal to increase signal to noise ratio

5.1.2.1 Thermoelastic and Ablative Regime

Nondestructive evaluation strives to evaluate a structure or material without damaging it. Depending on the technique, minor damages to the specimens can be necessary and is often admitted. It depends on the specific application, if these are acceptable

or not. While thermoelastic excitation is known to be nondestructive, excitation in the ablative regime can be compared to laser drilling. After excitation in the ablative regime a visible damage on the specimen with the spatial form of the laser source is visible. Fig. 5.8 shows a photography of the surface of a the steel specimen after ablative excitation.

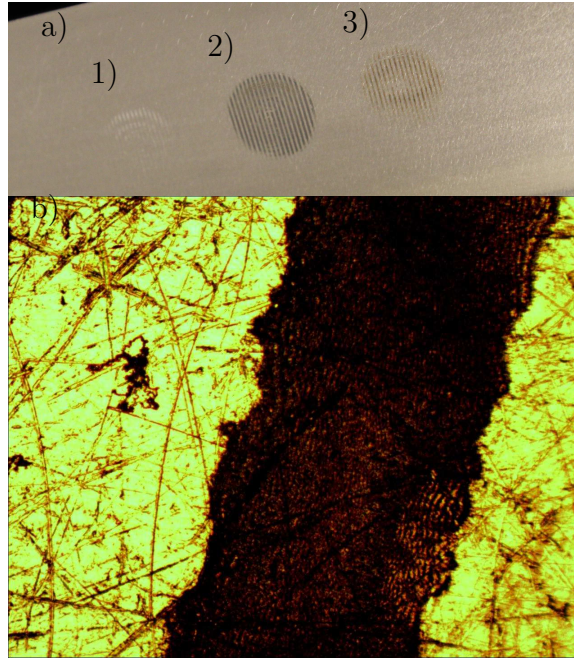


Figure 5.8: Ablation damage on steel a) for 1.) a single laser pulse, 2.) 256 pulses, 3.) 32 pulses. b) microscope picture ($200\times$ magnification of the damage after 256 pulses).

For thermoelastic excitation, neutral phase filters are used to attenuate the intensity of the laser beam. Unfortunately the signals measured in the thermoelastic regime were very low with a hardly detectable second harmonic. For the diffraction optic set-up, it is possible to increase the signal by using an oil coating. Due to the unsteady thermal expansion of the oil it is not possible to have repeatable results. In order to detect the second harmonic high laser power is used. The resulting signal excitation is ablative. The amplitude of the excited signal is about ten times larger

then the thermoelastic signal but has several drawbacks, described in section 3.2.4. Furthermore due to the removal of surface material the surface conditions change. This results in a material dependent change of the absorption ability. The signal strength increases about twice from the first to the second shot and develops cumulative for every further shot. In Fig. 5.9, the amplitude of the first and second harmonic increase with increasing number of shots and decreases after about 200 – 250 shots again. In the area of $\sim 150 - 250$ the source produces constant signals in A_1 and A_2 .

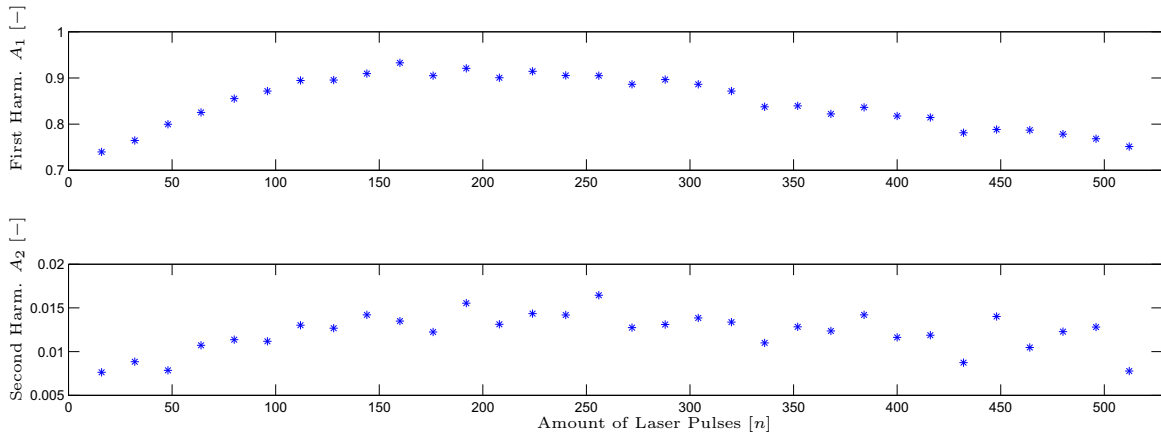


Figure 5.9: Excitation behavior of the first and second harmonic component against number of laser pulses on steel.

The behavior is different in aluminum. The amplitude increases almost constantly. In Fig. 5.10 the behavior of the ablative source on aluminum shows a linearly increasing behavior for the first harmonic amplitude. The signal is averaged for 16 signals for which the amplitude are almost constant. For the second harmonic the curve is different as the excitation of the second harmonic seems to increase strongly after ~ 200 pulses. Measurements on aluminum should be taken and averaged for $1 \leq n \leq 200$ and should stay in a relatively small range for averaged signals. Most of the results presented in the next section are averaged for 32 signals, starting after 2 – 5 laser pulses.

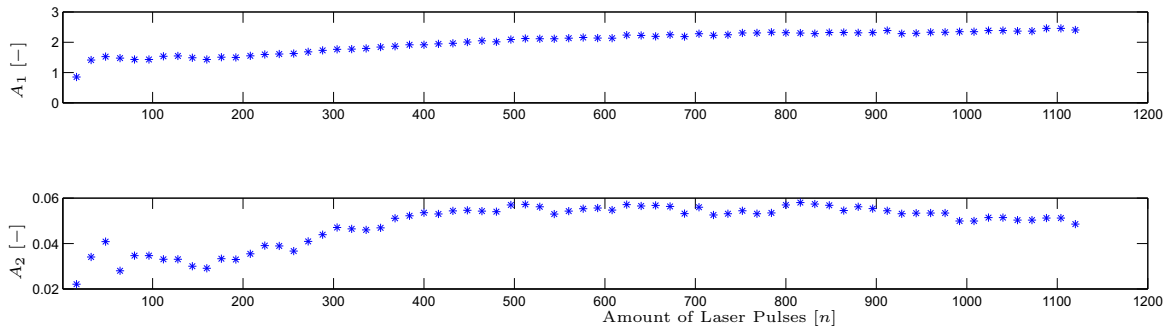


Figure 5.10: Excitation behavior of the first and second harmonic component against number of laser pulses on aluminum.

5.2 Measurement of the Nonlinearity of materials

Aluminum-Specimen The nonlinearity of the material is measured by exciting the Rayleigh wave signal in different propagation distances from the detecting wedge transducer which was clamped on the far side of the specimen. For aluminum specimen (Section 4.4) the nonlinearity parameter β showed an increasing trend with increasing propagation distance in all measurements for averaging on the first 32 signals. For the nine measurements taken on the same aluminum plate in similar conditions about 70% show an increasing second harmonic component in the signal. It shall be noticed that the difference to the other measurements can result from the difficulties in attaching the wedge transducer onto the plate in central positions.

For 7 out of ten measurements on the same aluminum plate the second harmonic amplitude is cumulative against the propagation distance in the farfield. In Fig. 5.11 the second harmonic starts to increase after about 9 cm. The slope of the A_2/A_1^2 -plot is the indicator for the nonlinearity of the material.

Fig. 5.12 shows the results from a single measurement procedure for several averages with different number of shots. The slopes of the best linear fit for the measurements is in a narrow range for the three measurements for consecutive averaged signals and confirms expectations from the results in Fig. 5.10. Measurements on

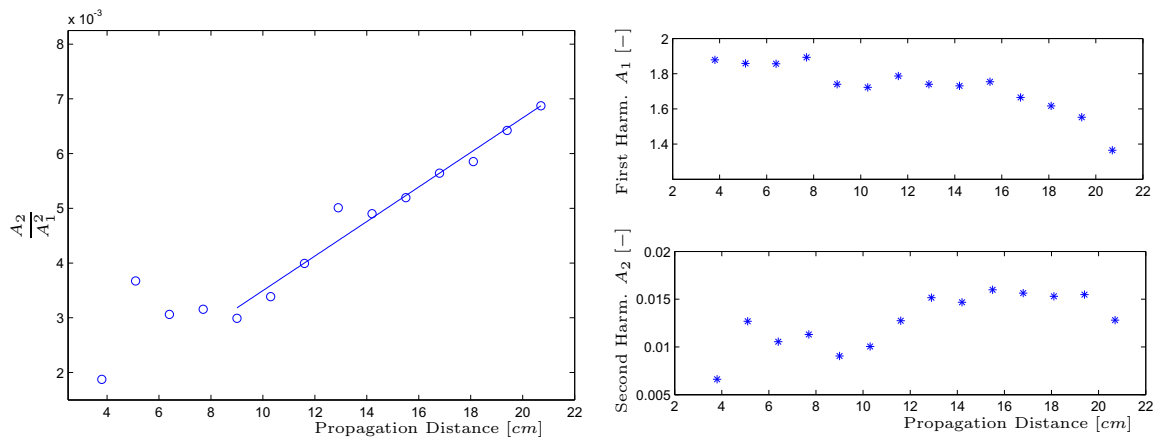


Figure 5.11: Development of the nonlinearity parameter and the first and second harmonic amplitudes on aluminum.

aluminum for averaging in a range of higher number of pulses (Fig. 5.10) did not show an increasing second harmonic anymore and can be described with the nonconstant excitation behavior after about two hundred pulses. The slopes vary between $8.66 \cdot 10^{-4}$ and $10.5 \cdot 10^{-4}$.

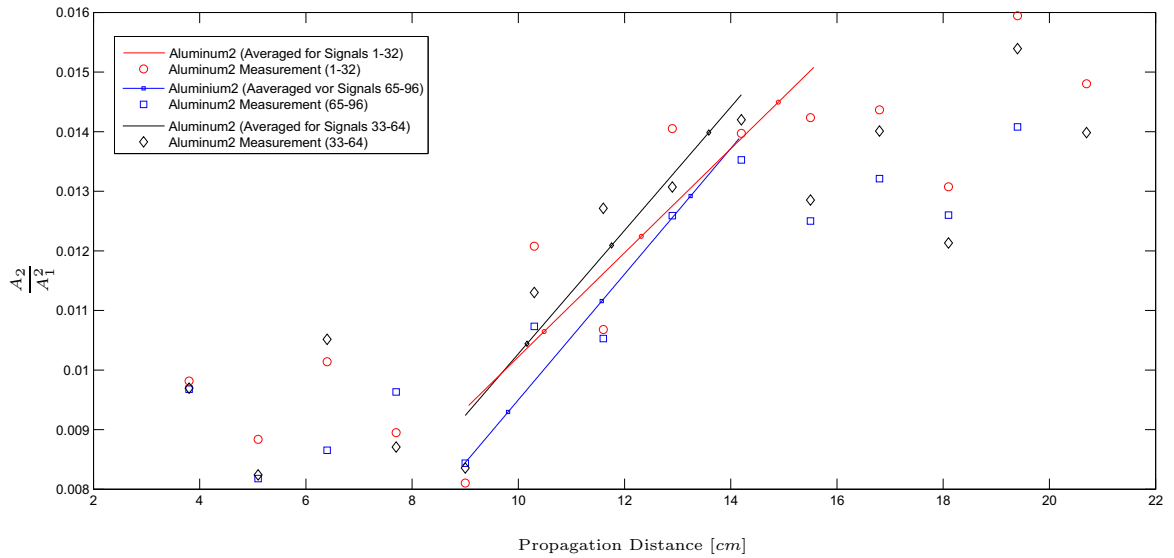


Figure 5.12: Nonlinearity measurement on aluminum averaged for different number of pulses.

In Fig. 5.13 the best linear fit for different measurements which were taken in constant conditions are shown. For the different measurements the receiving transducer was moved. This explains the differences in the absolute values for the measurements of the nonlinearity parameter and is not of further importance, as the nonlinearity of a material is described by the slope of the linear behavior of $A_2/A_1^{\text{②}}$ against the propagation distance. All the measurements had cumulative second harmonic wave forms and the slopes are within the range of $3.6 \cdot 10^{-4}$ and $12.4 \cdot 10^{-4}$ (Tab. 5.1).

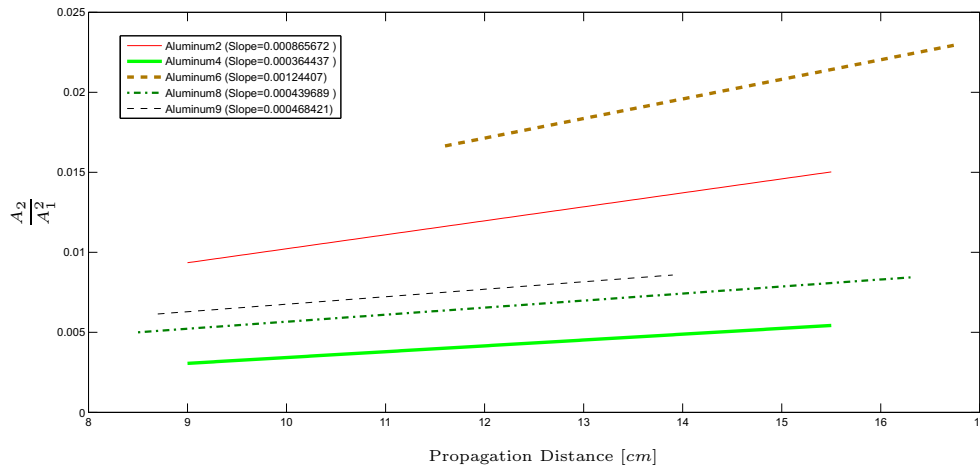


Figure 5.13: Best linear fit for nonlinearity measurements showing similar slopes.

Table 5.1: Measurement of nonlinearity of the aluminum plate

Measurement Set	Slope [$10^{-4}/cm$]	Deviation of average
Aluminum2	8.65672	1.892142
Aluminum4	3.64437	-3.120208
Aluminum6	12.4407	5.676122
Aluminum8	4.39689	-2.367688
Aluminum9	4.68421	-2.080368

Steel-Specimen For the measurements on the steel specimen it was not possible to detect an increase in the second harmonic. However for some measurements a cumulative nonlinearity was detectable. The lack of repeatability of the results may be explained by the fact that the the ablative source on steel is not constant enough (Fig. 5.9) or by the different surface conditions between each set of measurements when a surface treatment is necessary after the damage by ablative excitation. Fig. 5.14 shows the results for cumulative nonlinearity. Even though some measurements showed an increasing linearity it was not possible to detect a general trend of the materials behavior. In conclusion, the excited signal is too low in amplitude to detect the materials nonlinearity on steel compared to conventional contact transducer techniques[78].

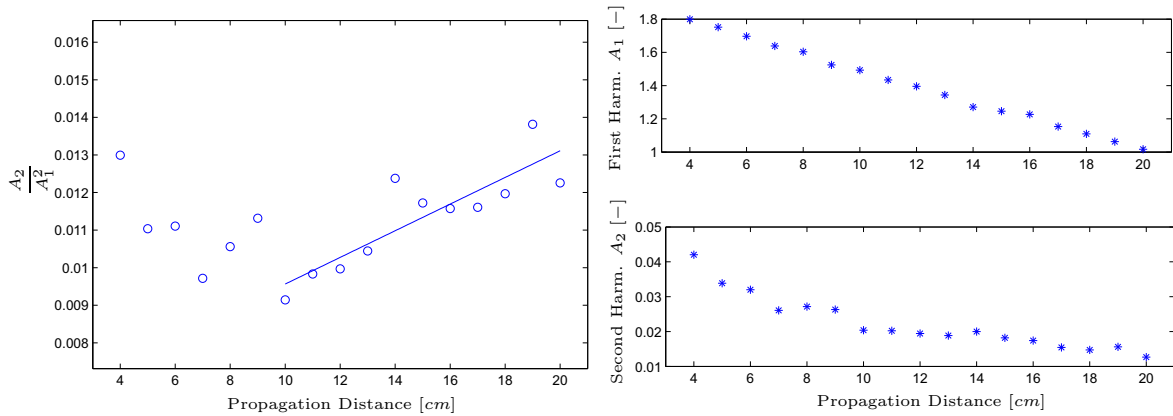


Figure 5.14: Nonlinearity measurement on steel. Shown is the development of the nonlinearity parameter and the behavior of the first and second harmonic amplitude.

CHAPTER VI

CONCLUSION

The results in the previous chapters show, that with the available optical equipment it is possible to excite a narrowband surface wave for nonlinearity measurements of materials. The set-up for diffraction optics enable the excitation of a narrowband tone burst with a very high center amplitude due to a non uniform energy distribution of the energy maxima on the specimen's surface. The use of a more advanced optical set up is questionable. [40] excited narrowband harmonic signals in the thermoelastic regime, which is found to excite insufficient signal strength for the purpose of the nonlinearity measurements considered in this research. While the pulse energy for the diffraction set up is limited by the power density damage threshold of the gratings, the use of lenticular arrays might be more conceivable due to the higher power thresholds of this optical method. Shadow masks offer the possibility for almost unlimited optical energy use, and are simple to align. Using cardboard as mask material offers a sufficient basis for the mask prototypes which are used in the experiments for the nonlinear measurements. However it is very likely that more precisely manufactured masks made of a more suitable material will increase the quality of the excitation and the repeatability of the optical source. Masks made of ceramics might have a better resistance against the damage from the laser illumination than exhibited by the cardboard. Furthermore, ceramics are very stiff and can be fabricated very accurately for small feature sizes, while cardboard tends to deform when formed in small thin structures.

This research shows that the harmonic source in the ablative regime excites a predictable nonlinear signal in the nearfield of the source. This conclusion matches

those of other authors[75, 39, 28]. At larger distances in the farfield from the source ($\sim 8 - 9 \text{ cm}$), the measured signal is useful for making nonlinear measurements. The measurement results made on a plate of aluminum showed good repeatability of the characterization of the material's nonlinearity. The ablative source on aluminum showed a consistent character for a wide range of laser pulses. After about 200 – 250 laser pulses the excitation of the second harmonic frequency increases, and the sources are repeatable and consistent enough to be used for nonlinear measurements. However, the ablative source on a steel specimen showed variations in the excitation of the first and second harmonic amplitude. This inconsistent character of the optical source in steel gives unacceptably high variations in the measurement of the nonlinearity parameter.

According to these results, it is questionable if the laser generation in the ablative regime can be adapted for field measurements. The material dependency and surface damage restrict the application to distinct materials and structures. The main reason to choose an ablative excitation regime is the high ultrasonic signal amplitudes when compared to those from the thermoelastic regime. Several authors discussed ways to increase the signal strength of the ultrasonic signal from a laser source without damaging the surface. This signal can be increased by applying an absorbing layer on the specimen[6, 76, 72, 18]. Laser illumination of the sacrificial layer will evaporate the layer material and the resulting normal force can excite an elastic surface wave, stronger than the thermoelastic excited wave. But even for the ablative regime, the excited ultrasonic signal is relatively low in general. The literature discusses several ways to increase the signals strength of laser ultrasonics in general. Constraining the source surface [22] increases the amplitude as well as the use of laser radiation of short wave lengths [74] and acousto optic modulation[65].

Another way to improve the laser excitation possibility might be the excitation of a larger amount of sources. The laser beam could be divided on a large amount of

optical fibers, which are only capable of low laser powers[23, 43, 42]. These could be used to form a uniform pattern for narrowband generation with a very high number of cycles.

Appendix

Divergence Theorem

$$\int_A \tau_{kl} n_k dA = \int_V \tau_{kl,k} dV \quad (\text{A.1})$$

Kronecker-Delta

$$\delta_{ij} = \begin{cases} 1, & \text{for } j = i \\ 0, & \text{else} \end{cases} \quad (\text{A.2})$$

Additional equations for the derivation of the thermoelastic source[3]

$$V^R(x_3) = d_1 e + d_2 e^{-qx_3} \quad (\text{A.3})$$

$$W^R(x_3) = d_3 e + e^{-qx_3} \quad (\text{A.4})$$

with

$$d_1 = -\frac{1}{2} \frac{k_R^2 + q^2}{k_R p}, d_2 = \frac{q}{k_R}, d_3 = \frac{1}{2 \frac{k_R^2 + q^2}{k_R^2}} \quad (\text{A.5})$$

and

$$p^2 = k_R^2 - \frac{\omega^2}{c_L^2}, q^2 = k_R^2 - \frac{\omega^2}{c_T^2}. \quad (\text{A.6})$$

A defines the amplitude of a surface wave, the relevant stresses are

$$\tau_{11} = AT_{11}^R(x_3)\phi(x_1, x_2) - A \frac{\mu}{k_R} V^R(x_3) \frac{\partial^2 \phi}{\partial x_2^2} \quad (\text{A.7})$$

$$\tau_{3\beta} = AT_{3\beta}^R(x_3) \frac{1}{k_R} \frac{\partial \phi}{\partial x_2^2} \quad (\text{A.8})$$

$$\tau_{33} = AT_{33}^R(x_3)\phi \quad (\text{A.9})$$

where

$$T_{11}^R(x_3) = \mu[d_4e^{-px_3} + d_5e^{-qx_3}] \quad (\text{A.10})$$

$$T_{3\beta}^R(x_3) = \mu[d_6e^{-px_3} + d_7e^{-qx_3}] \quad (\text{A.11})$$

$$T_{33}^R(x_3) = \mu[d_8e^{-px_3} + d_9e^{-qx_3}] \quad (\text{A.12})$$

with

$$d_4 = \frac{1}{2}(k_R^2 + q^2) \frac{2p^2 + k_R^2 - q^2}{pk_R^2}, d_5 = -2q, d_6 = \frac{k_R^2 + q^2}{k_R}, d_7 = -\frac{k_R^2 + q^2}{k_R}, d_8 = -\frac{1}{2} \frac{(k_R^2 + q^2)^2}{pk_R^2}, d_9 = 2q \quad (\text{A.13})$$

$$I = \int_0^\infty [T_R^{11}(x_3)V^R(x_3) - T_R^{13}(x_3)W^R(x_3)] dx_3 \quad (\text{A.14})$$

Substitution of the expression for the relevant displacements it follows

$$I = \mu J \quad (\text{A.15})$$

with the negative constant $J[3]$.

REFERENCES

- [1] ACHENBACH, J. D., “Lamb waves as thickness vibrations superimposed on a membrane carrier wave,” *J. Acoust. Soc. Am.*, vol. 103, pp. 2283–2286, 1998.
- [2] ACHENBACH, J. D., *Wave Propagation in Elastic Solids*. Elsevier, first ed., 1999.
- [3] ACHENBACH, J. D., “Calculation of surface wave motions due to a subsurface point force: An application of elastodynamic reciprocity,” *J. Acoust. Soc. Am.*, vol. 107, pp. 1892–1897, 2000.
- [4] ACHENBACH, J. D., “Laser excitation of surface wave motion,” *J. Mech Phys. Solids*, vol. 51, pp. 1885–1902, 2003.
- [5] ACHENBACH, J. D., “The thermoelasticity of laser-based ultrasonics,” *Journal of Thermal Stresses*, vol. 28, pp. 713–727, 2005.
- [6] AINDOW, A. M., DEWHURST, R. J., HUTCHINS, D. A., and PALMER, S. B., “Laser-generated ultrasonic pulses at free metal surfaces,” *J. Acoust. Soc. Am.*, vol. 69, pp. 449–455, 1981.
- [7] AINDOW, A. M., DEWHURST, R. J., and PALMER, S. B., “Laser-generation of directional surface acoustic wave pulses in metals,” *Optics Communications*, vol. 42, pp. 116–120, 1982.
- [8] ARIAS, I. and ACHENBACH, J. D., “Thermoelastic generation of ultrasound by line-focused laser irradiation,” *International Journal of Solids and Structures*, vol. 40, pp. 6917–6935, 2003.
- [9] ASH, E. A., DIEULESAINT, E., and RAKOUTH, H., “Generation of surface acoustic waves by means of a cw laser,” *Electron. Lett.*, vol. 16, pp. 470–472, 1980.
- [10] AUSELL, J., BRUN, A. L., and BABOUX, J., “Generating acoustic waves by laser: theoretical and experimental study of the emission source,” *Ultrasonics*, vol. 26, pp. 245–255, 1988.
- [11] BABY, S., KOWMUDI, B. N., OMPRAKASH, C. M., SATYANARAYANA, D. V. V., BALASUBRAMANIAM, K., and KUMAR, V., “Creep damage assessment in titanium alloy using a nonlinear ultrasonic technique,” *Scripta Materialia*, vol. 59, pp. 818–821, 2008.

- [12] BARNARD, D. J., BRASCHE, L. J. H., RAULERSON, D., and DEGTYAR, A. D., “Monotonic fatigue damage accululation with Rayleigh wave harmonic generation measurements,” *Review of Progress In Quantitative Nondestructive Evaluation*, vol. 22, pp. 1393–1400, 2003.
- [13] BERNSTEIN, J. and SPICER, J., “Line source representation for laser-generated ultrasound in aluminium,” *J. Acoust. Soc. Am*, vol. 107, pp. 1352–1357, 2000.
- [14] BLACKSHIRE, J. L., SATHISH, S., NA, J., and FROUIN, J., “Nonlinear laser ultrasonic measurements of localized fatigue damage,” *Review of Progress In Quantitative Nondestructive Evaluation*, vol. 22, pp. 1479–1488, 2003.
- [15] BLEANEY, B. I. and BLEANEY, B., *Electricity and Magnetism*. Oxford University Press, second ed., 1965.
- [16] CARSLAW, H. S. and JAEGER, J., *Conductivity of Heat in Solids*. Clarendon, first ed., 1959.
- [17] CASH, W. and CAI, W., “Dislocation contribution to acoustic nonlinearity: The effect of orientation-dependent line energy,” *J. Appl. Phys.*, vol. 109, 2011.
- [18] CHENG, J. C. and ZHANG, S. Y., “Quantitative theory for laser-generated Lamb waves in orthotropic thin plates,” *Appl. Phys. Lett.*, vol. 74, pp. 2087–2089, 1999.
- [19] CHRISTIAN, E., “Experimental characterization of creep damage using the non-linearity ultrasonic technique,” Master’s thesis, Georgia Institute of Technology, 2011.
- [20] COSENZA, C., KENDERIAN, S., DJORDJEVIC, B. B., GREEN, R. E., and PASA, A., “Generation of Narrowband Antisymmetric Lamb Waves Using a Formed Laser Source in the Ablative Regime,” *IEEE*, vol. 54, pp. 147–156, 2007.
- [21] COSTLEY, R. D., *Laser Generation of Rayleigh and Lamb Waves for Ultrasonic Nondestructive Testing*. PhD thesis, Georgia Institute of Technology, 1993.
- [22] DEWHURST, R. J., HUTCHINS, D. A., PALMER, S. B., and SCRUBY, C. B., “Quantitative measurements of lasergenerated acoustic waveforms,” *J. Appl. Phys.*, vol. 53, pp. 4064–4071, 1982.
- [23] DI SCALEA, F. L., PRENDT, T. P., SPICER, J. B., and DJORDJEVIC, B. B., “Remote laser generation of narrow-band surface wave through optical fibers,” *J. Acoust. Soc. Amer.*, vol. 34, pp. 2527–2531, 1999.
- [24] DIAZ, E., “Email conversation 05/31/12.”
- [25] DIXON, S., HARRISON, T., FAN, Y., and PETCHER, P. A., “Thermoelastic laser generated ultrasound using a ring source,” *J. Phys. D: Appl. Phys.*, vol. 45, p. 7pp, 2012.

- [26] DOYLE, P. A. and SCALA, C. M., “Near-field ultrasonic Rayleigh waves from a laser line source,” *Ultrasonics*, vol. 34, pp. 1–8, 1996.
- [27] FASSBENDER, S., HOFFMANN, B., and ARNOLD, W., “Efficient generation of acoustic pressure waves by short laser pulses,” *Mat. Sci. Eng.*, vol. 122, pp. 37–41, 1989.
- [28] FRASS, A., LOMONOSOV, A., and HESS, P., “Investigation of phase transition thresholds by nonlinear transient laser gratings on silicon surfaces,” *J. Appl. Phys.*, vol. 87, pp. 3505–3510, 2000.
- [29] FREDERIK, D., “Damage detection in concrete using diffuse ultrasound measurements and an effective medium theory for wave propagation in multi-phase materials,” Master’s thesis, Georgia Institute of Technology, 2009.
- [30] GOSPODYN, J. P., SARDARLI, A., BRODNIKOVSKI, A. M., and FEDOSEJEVS, R., “Ablative generation of surface acoustic waves in aluminium using ultraviolet laser pulses,” *Journal of Applied Physics*, vol. 29, pp. 564–571, 2002.
- [31] GRAF, T., *Laser: Grundlagen der Laserstrahlquellen*. Vieweg+Teubner, first ed., 2009.
- [32] HAMILTON, M. F. and BLACKSTOCK, D. T., *Nonlinear Acoustics*. Elsevier Academic Press, first ed., 1998.
- [33] HARATA, A., NISHIMURA, N., and SAWADA, T., “Laser-induced surface acoustic-waves and photothermal surface gratings generated by crossing 2 pulsed laser-beams,” *Appl. Phys Lett.*, vol. 57, pp. 132–134, 1990.
- [34] HARIHARAN, P., *Basics of Interferometry*. Elsevier Academic Press, second ed., 2007.
- [35] HECHT, E., *Theory and Problems of Optics*. McGraw-Hill Book Company, first ed., 1975.
- [36] HERRMANN, J., KIM, J., JACOBS, L. J., QU, J. M., LITTLES, J. W., and SAVAGE, M. F., “Assessment of material damage in a nickel-base superalloy using nonlinear Rayleigh surface waves,” *J. Appl. Phys.*, vol. 99, 2006.
- [37] HIRTH, J. P. and LOTHE, J., *Theory of dislocations*. John Wiley & Sons, Inc., second ed., 1982.
- [38] HOFFMANN, A. and ARNOLD, W., “Calculation and measurement of the ultrasonic signals generated by ablating material with a q-switched pulse laser,” *Applied Surface Science*, vol. 96-98, pp. 71–75, 1996.
- [39] HROVATIN, R. and MOZINA, J., “Optodynamic aspect of pulsed laser ablation process,” *Applied Surface Science*, vol. 86, pp. 213–218, 1995.

- [40] HUANG, J., KISHNASWAMY, S., and ACHENBACH, J. D., “Laser generation of narrow-band surface waves,” *J. Acoust. Soc. Amer.*, vol. 34, pp. 2527–2531, 1992.
- [41] HURLEY, D. H. and SPICER, J. B., “Point-source representation for laser-generated ultrasound in an elastic, transversely isotropic half-space,” *J. Appl. Phys.*, vol. 86, pp. 3423–3427, 1999.
- [42] JARZYNSKI, J. and BERTHELOT, Y., “The use of optical fibers to enhance the laser generation of ultrasonic waves,” *J. Acoust. Soc. Am.*, vol. 85, pp. 158–162, 1989.
- [43] KENDERIAN, S., DJORDJEVIC, B. B., and R. E. GREEN, J., “Point and source laser generation of ultrasound for inspection of internal and surface flaws in rail and structural materials,” *Res. Nondestr. Eval.*, vol. 13, pp. 189–200, 2001.
- [44] KENDERIAN, S., DJORDJEVIC, B. B., and R. E. GREEN, J., “Narrow band laser-generated surface acoustic waves using a formed source in the ablative regime,” *J. Acoust. Soc. Am.*, vol. 113, pp. 261–266, 2003.
- [45] KHAN, A. S. and HUANG, S., *Continuum Theory of Plasticity*. John Wiley & Sons, Inc., first ed., 1995.
- [46] KIM, H., JHANG, K., SHIN, M., and KIM, J. 2005.
- [47] KIM, J.-Y., JACOBS, L. J., and QU, J., “Experimental characterization of fatigue damage in a nickel-base superalloy using nonlinear ultrasonic waves,” *J. Appl. Phys.*, vol. 120, pp. 1266–1273, 2006.
- [48] KREHL, P., SCHWIRZKE, F., and COOPER, A. W., “Correlation of stress-wave profiles and the dynamics of the plasma produced by laser irradiation of plane solid targets,” *J. Appl. Phys.*, vol. 46, pp. 4400–4406, 1975.
- [49] LEDBETTER, H. M. and MOULDER, J. C., “Laser-induced Rayleigh waves in aluminium,” *J. Acoust. Soc. Amer.*, vol. 34, pp. 2527–2531, 1979.
- [50] LIU, M., KIM, J.-Y., JACOBS, L. J., and QU, J., “Experimental study of nonlinear Rayleigh wave propagation in shot-peened aluminum plates-Feasibility of measuring residual stress,” *NDT&E International*, vol. 44, pp. 67–74, 2011.
- [51] LUXENBURGER, S. and ARNOLD, W., “Laser ultrasonic measurement in fatigue-damaged materials,” *Ultrasonics*, vol. 40, pp. 797–801, 2002.
- [52] MALVERN, L. E., *Introduction to the Mechanics of a Continuous Medium*. Prentice Hall, first ed., 1977.
- [53] MATTHIAS, S., “Finite element simulation of crack depth measurements in concrete using diffuse ultrasound,” Master’s thesis, Georgia Institute of Technology, 2011.

- [54] McDONALD, F. A., “On the precursor in laser-generated ultrasound waveforms in metals,” *Appl. Phys. Lett.*, vol. 56, pp. 230–232, 1990.
- [55] MCKIE, A. D. W., WAGNER, J. W., and J. B. SPICER, C. M. P., “Laser generation of narrow-band and directed ultrasound,” *Ultrasonics*, vol. 27, pp. 323–330, 1989.
- [56] MI, B. and UME, I. C., “Parametric studies of laser generated ultrasonic signals in ablative regime: Time and frequency domains,” *Journal of Nondestructive Evaluation*, vol. 21, pp. 23–33, 2002.
- [57] MURRAY, T. W., J. B. DEATON, J., and WAGNER, J. W., “Experimental evaluation of enhanced generation of ultrasonic waves using an array of laser sources,” *Ultrasonics*, vol. 34, pp. 69–77, 1996.
- [58] MURRAY, T. W. and WAGNER, J. W., “Experimental evaluation of enhanced generation of ultrasonic waves using an array of laser sources,” *J. Appl. Phys.*, vol. 85, pp. 2031–2040, 1999.
- [59] NAKANO, H. and NAGAI, S., “Laser generation of antisymmetric ultrasonic Lamb waves in thin plates,” *Ultrasonics*, vol. 29, pp. 230–234, 1991.
- [60] NAM, T., CHOI, S., LEE, T., JHANG, K.-Y., and KIM, C., “Acoustic non-linearity of narrowband laser-generated surface waves in the bending fatigue of al6061 alloy,” *Journal of the Korean Physical Society*, vol. 57, pp. 1212–1217, 2010.
- [61] NELSON, K. A., MILLER, R. J. D., LUTZ, D. R., and FAYER, M. D., “Optical-generation of tunable ultrasonic-waves,” *J. Appl. Phys.*, vol. 53, pp. 1144–1149, 1982.
- [62] NISHINO, H., TSUKAHARA, Y., NAGATA, Y., KODA, T., and YAMANAKA, K., “Excitation of high-frequency surface acoustic-waves by phase-velocity scanning of a laser interference fringe,” *Appl. Phys Lett.*, vol. 62, pp. 2036–2038, 1993.
- [63] O’SHEA, D. C., CALLEN, W. R., and RHODES, W. T., *Introduction to Lasers and Their Applications*. Addison-Wesley Publishing Company, first ed., 1977.
- [64] PANTANO, A. and CERNIGLIA, D., “Simulation of laser-generated ultrasonic wave propagation in solid media and air with application to nde,” *Appl. Phys. A*, vol. 98, pp. 327–336, 2009.
- [65] PIERCE, R., UME, C., and JARZYNSKI, J., “Temporal modulation of laser source for the generation of ultrasonic waves,” *Ultrasonics*, vol. 33, pp. 133–137, 1995.
- [66] PRUELL, C., KIM, J.-Y., and JACOBS, L. J., “Evaluation of plasticity driven material damage using Lamb waves,” *Appl. Phys. Lett.*, vol. 91, 2007.

- [67] READY, J. F., *Effects of High Power Laser Radiation*. New York: Academics, first ed., 1971.
- [68] ROSE, L. R. F., "Point-source representation for laser-generated ultrasound," *J. Acoust. Soc. Am.*, vol. 75, pp. 723–732, 1984.
- [69] ROYER, D. and CHENU, C., "Experimental and theoretical waveforms of Rayleigh waves generated by a thermoelastic laser line source," *Ultrasonics*, vol. 38, pp. 891–895, 2000.
- [70] ROYER, D. and DIEULESAINT, E., "Analysis of thermal generation of Rayleigh waves," *J. Appl. Phys.*, vol. 56, pp. 2507–2511, 1984.
- [71] SANDERSON, T., UME, C., and JARZYNSKI, J., "Laser generated ultrasound: a thermoelastic analysis of the source," *Ultrasonics*, vol. 35, pp. 115–124, 1997.
- [72] SCRUBY, C. B., "Some applications of laser ultrasound," *Ultrasonics*, vol. 27, pp. 195–209, 1989.
- [73] SCRUBY, C. B., DEWHURST, R. J., HUTCHINS, D. A., and PALMER, S. B., "Quantitative studies of thermally generated elastic waves in laserirradiated metals," *J. Appl. Phys.*, vol. 51, pp. 6210–6216, 1980.
- [74] SCRUBY, C. B. and DRAIN, L. E., *Laser Ultrasonics - Techniques and Applications*. Adam Hilger, first ed., 1990.
- [75] SHEN, Y.-C., LOMOSONOV, A., FRASS, A., and HESS, P., "Nonlinear surface acoustic waves launched by excitation of higher harmonics in transient laser gratings," *AIP Conference Proceedings*, vol. 463, pp. 418–420, 1999.
- [76] SHEN, Z. H., XU, B. Q., NI, X. W., LU, J., and ZHANG, S. Y., "Theoretical study om line source laser-induced surface acoustic waves in two-layer structure in ablative regime," *Optics and Laser Technology*, vol. 36, pp. 139–143, 2004.
- [77] SHULL, P. J., *Nondestructive Ecaluation - Theory, Techniques, and Applications*. Marcel Dekker, Inc. , New York, first ed., 2002.
- [78] SIMON, W., "Characterization of fatigue damage in A36 steel specimens using nonlinear Rayleigh surface waves," Master's thesis, Georgia Institute of Technology, 2011.
- [79] SPICER, J., *Laser ultrasonics in finite structures: comprehensive modelling with supporting experiment*. PhD thesis, The John Hopkins University, 1991.
- [80] STEEL, W. H., *Interferometry*. Cambridge University Press, second ed., 1983.
- [81] TANAKA, T. and IZAWA, Y., "Nondestructive detection of small internal defects in carbon steel by laser ultrasonics," *Jpn. J. Appl. Phys.*, vol. 40, pp. 1477–1481, 2001.

- [82] THORLABS, “Nir transmission gratings.” Website. [http :
//www.thorlabs.com/NewGroupPage9.cfm?ObjectGroupID = 1782.](http://www.thorlabs.com/NewGroupPage9.cfm?ObjectGroupID=1782)
- [83] TREIBER, M., “Characterization of cement-based multiphase materials using ultrasonic wave attenuation,” Master’s thesis, Georgia Institute of Technology, 2008.
- [84] VALLURI, J. S., BALASUBRAMANIAM, K., and PRAKASH, R. V., “Creep damage characterization using non-linear ultrasonic techniques,” *Acta Materialia*, vol. 58, pp. 2079–2090, 2010.
- [85] VIKTOROV, I., *Rayleigh and Lamb Waves, Physical Theory and Applications*. Plenum Press New York, first ed., 1967.
- [86] VON GUTFELD, R. J., “Thermoelastic generation of elastic waves for non-destructive testing and medical diagnostics,” *Ultrasonics*, pp. 175–182, 1980.
- [87] WHITE, R. M., “Generation of elastic waves by transient surface heating,” *J. Appl. Phys.*, vol. 56, pp. 2507–2511, 1962.
- [88] ZABOLOTSKAYA, E., “Nonlinear propagation of plane and circular Rayleigh waves in isotropic solids,” *J. Acoust. Soc. Am.*, vol. 91, pp. 2569–2575, 1992.